Unterschrift der Betreuerin

Diplomarbeit

Flavor non-universal Z' at the LHC

Ausgeführt am
Atominstitut der Technischen Universität Wien
in Verbindung mit dem
Institut für Hochenergiephysik der Österreichischen Akademie der Wissenschaften

unter der Leitung von

Univ.-Doz. Dr. techn. Dipl.-Ing. Claudia-Elisabeth Wulz

und

Dr. Suchita Kulkarni

durch

Gerhard Ungersbäck
e1125440

Felberstraße 58/11-12
1150 Wien

Wien, am 24. Juli 2020

Unterschrift

Abstract

Z' bosons arise in various models of physics beyond the Standard Model. In this thesis, a lepton flavor non-universal Z' extension is studied at the LHC. In the context of dark matter searches, a simplified model in which the Z' boson couples only to leptons of the Standard Model particle content (leptophilic) was proposed. It was shown that loop induced couplings provide sufficiently large couplings to colored states to study this extension in the Drell-Yan process at the LHC. The henceforth studied Z' boson couples at tree-level to electrons, muons and to neutrinos as required by gauge invariance. The model is reviewed and furthermore the importance of interference terms is discussed. LEP bounds on contact operators tightly constrain lepton couplings to Z' bosons. The bounds are derived and the dependency of allowed couplings to muons for a fixed coupling to electrons are presented. Z' parameter points are excluded with the publicly available code ZPEED. ZPEED allows for exclusion in Drell-Yan processes from experimental data collected by the ATLAS collaboration with 139 fb^{-1}. It was recently published and validated by comparison to limits obtained by experimental searches. The approach taken by ZPEED is reviewed and the statistical analysis of dilepton invariant mass distributions is extended by considering the ratio of the dilepton invariant mass spectrum of the electron and muon channel. Ratios are cleaner observables, since theoretical uncertainties in the background prediction cancel. Both analysis methods are compared for the studied parameter space. Finally, the analysis is also performed on a generic Z' model with tree-level couplings to quarks.

Kurzfassung

Z' Bosonen werden in verschiedenen Erweiterungen des Standardmodells der Teilchenphysik vorhergesagt. In dieser Arbeit wird ein lepton flavor non-universal Z' Modell am LHC untersucht. Diese Erweiterung, in der das Z' Boson nur mit Leptonen des Standardmodells wechselwirkt (leptophil), wurde im Rahmen von Suchen nach dunkler Materie vorgeschlagen. Es wurde gezeigt, dass loop-induzierte Wechselwirkungen mit Quarks ausreichend stark sind um dieses Modell im Drell-Yan Prozess am LHC zu untersuchen. Das im Folgenden untersuchte Z' Boson wechselwirkt in erster Ordung mit Elektronen, Myonen und weiters mit Neutrinos um die Eichinvarianz des Standardmodells nicht zu verletzen. Die Berechung der induzierten Wechselwirkung wird rekaptituliert und weiters wird die Relevanz von Interferenzeffekten aufgezeigt. Limits von LEP auf Kontaktoperatoren beschränken die erlaubten Wechselwirkungen von Z' Bosonen mit Leptonen. Die Limits werden hergeleitet und die Abhängigkeit von noch nicht ausgeschlossener Kopplungsstärke zu Myonen, bei angenommener Kopplungstärke zu Elektronen, präsentiert. Parameterpunkte des Z' Modells werden mittels dem öffentlichen Programm ZPEED analysiert. ZPEED verwendet 139 fb^{-1} an Drell-Yan-Ereignissen der ATLAS collaboration. Die von ZPEED verwendete Methode wird erläutert und die statistische Auswertung in Zerfällen in Elektronen und Myonen wird erweitert, bei Betrachtung von deren Verhältnis. Der Vorteil der letztgenannten Methode ist, dass theoretische Unsicherheiten in dem Hintergrundprozess wegfallen. Zum Abschluss wird die Analyse auf ein generisches Z' Modell angewandt, in welchem die Z' Kopplung an Quarks nicht durch Wechselwirkungen von Leptonen verursacht wird.

Contents

1. Introduction

The Standard Model of particle physics (SM) provides an accurate description of nature at the subatomic scale. It is a quantum field theory with gauge group $SU(3)_C \times SU(2)_L \times U(1)_Y$, which is spontaneously broken by the Higgs mechanism. The theory is lepton flavor universal, which means that all leptons couple with the same strength to mediator particles. The only exception is the coupling to the Higgs particle which is very small because of the low lepton masses.

In this thesis, a lepton flavor non-universal Z' extension to the SM is studied. Z' bosons arise in various models of physics beyond the Standard Model, see [1] for a recent review. Z' bosons refer to massive, electrically neutral vector bosons without color interaction, as the Standard Model Z boson. It is also under consideration as a possible portal to dark matter. Dark matter accounts for about 26% of the content of our universe and so far no direct evidence has been found. Measurements of cosmic rays [2] by PAMELA, FERMI and AMS-02 drew attention to leptophilic portals, since an excess in the positron spectrum has been found. In this context a leptophilic flavor non-universal Z' model was introduced with an additional dark matter particle [3]. It was shown that, through loop induced couplings, resonance searches at the LHC for this leptophilic Z' particle are feasible. The publication discusses cases in which the Z' particle couples at tree-level only to one lepton species (μ or τ) and an additional dark matter particle. In this thesis the model is adjusted to couple to electrons, muons and neutrinos as required by gauge invariance of the Standard Model. No dark matter particle is introduced. By combining both search channels in the Drell-Yan process, parameter points are excluded. Special attention is drawn to the ratio of the dilepton invariant mass spectrum of the electron and muon channel, since it is a theoretically cleaner observable than the spectra itself. The ratio of the differential cross sections of the two channels has also been proposed as a test of lepton flavor universality [4]. An advantage of the leptophilic model is a reduced parameter space, since it only consists of the couplings to electrons and muons and the Z' mass. Only one additional parameter, the scale at which the couplings to quarks is zero, is necessary to specify signals at hadron colliders. The analysis is also performed on a generic Z' model with tree-level couplings to quarks.

This thesis is organized as follows: Section 2 introduces the Standard Model of particle physics. The particle content and the gauge groups are discussed and furthermore the renormalization group equation. In section 3 the leptophilic flavor non-universal Z' model with loop induced couplings to quarks, introduced in [3] is reviewed and possible search scenarios at hadron colliders are discussed. The parameter space of the model is studied and interference effects are analysed. This section concludes with the reinterpretation of existing bounds from LEP and limits from anomalous magnetic moment measurements and $Z - Z'$ mixing. In section 4 the deployed ZPEED code is introduced. It allows for Z' model exclusions with experimental data from the ATLAS collaboration with 139 fb^{-1}. The statistical evaluation is discussed and the exclusion based on the ratio of the dilepton invariant mass spectrum of the electron and muon channel is explained. In section 5 the obtained results are presented. Section 6 concludes the present work.

2. The Standard Model of particle physics

Elementary particles and forces are successfully described by quantum field theory. The only known exception are gravitational interactions, for which no formulation on quantum level has been found yet. In this chapter the basics of quantum field theory are covered to further introduce the Standard Model of particle physics. For a detailed treatment of this rich subject please see references [5] or [6], which are also the source for what follows.

2.1. Quantum field theory

In the formulation of quantum field theory elementary matter particles are described by spin-1/2 particles (fermions) and mediators of forces by spin-0 or spin-1 particles (bosons). Quantum field theory combines quantum mechanics and special relativity. Therefore, the space-time symmetries are given by Lorentz transformations. The spin number of the particle specifies its transformation properties under Lorentz transformations. According to Noether's theorem, to every continuous symmetry transformation corresponds a conserved current. The corresponding conserved charges of space-time symmetries are: energy conservation, momentum conservation and angular momentum conservation.

2.1.1. Introduction: Quantum electrodynamics

This section introduces some concepts of elementary particle physics, starting with free fields and concluding with interactions in the framework of quantum electrodynamics (QED).

Free fermions

Fermions with mass m are described by 4-component Dirac spinors ψ. Their equation of motion (e.o.m.) is the Dirac equation $(i\partial\!\!\!/ - m)\psi = 0$. The Lagrangian is given by

$$\mathcal{L} = \overline{\psi}(i\partial\!\!\!/ - m)\psi, \quad \text{where} \quad \overline{\psi} = \psi^\dagger\gamma^0, \quad \partial\!\!\!/ = \gamma^\mu\partial_\mu, \tag{2.1}$$

which gives the Dirac equation by minimizing the action functional via $\delta_{\bar{\psi}} \int dx^4 \mathcal{L} = 0$. The matrices γ are a representation of the Dirac algebra $\{\gamma^\mu, \gamma^\nu\} = 2g^{\mu\nu}$. Additionally to the space-time transformation, the equation contains a symmetry regarding global phase transformations:

$$\psi(x) \to e^{-i\alpha}\psi(x). \tag{2.2}$$

This yields the conserved current $j^\mu = \overline{\psi}\gamma^\mu\psi$, whose conserved charge is conservation of electrical charge.
In the Weyl representation, the γ matrices are given by

$$\gamma^0 = \begin{pmatrix} 0 & 1 \\ 1 & 0 \end{pmatrix}, \quad \gamma^i = \begin{pmatrix} 0 & \sigma^i \\ -\sigma^i & 0 \end{pmatrix}, \quad \to \gamma^\mu = \begin{pmatrix} 0 & \sigma^\mu \\ \overline{\sigma}^\mu & 0 \end{pmatrix}. \tag{2.3}$$

Thus, fermions can also be described by two 2-component Weyl spinors ψ_L and ψ_R, defined as $\psi = (\psi_L\ \psi_R)^T$. These spinors, are solutions to two differential equations coupled by the mass term, equivalent to the Dirac equation. In this formulation the Dirac Lagrangian is given by

$$\mathcal{L} = i\overline{\psi}_L\overline{\sigma}^\mu\partial_\mu\psi_L + i\overline{\psi}_R\sigma^\mu\partial_\mu\psi_R - m(\overline{\psi}_R\psi_L + \overline{\psi}_L\psi_R) \tag{2.4}$$

where $\overline{\psi} = (\psi_R^\dagger\ \psi_L^\dagger) = (\overline{\psi}_R\ \ \overline{\psi}_L)$.

Free bosons

Massless free bosons with spin 1 are described by a 4-component relativistic wave function A_μ, a solution of $\left(\partial^2 g^{\mu\nu} - \partial^\mu\partial^\nu\right) A_\nu = 0$. Solutions to this equation have gauge freedom, meaning that a solution has infinitely many equivalent solutions which are connected via the gauge transformation $A_\mu \to A_\mu + \partial_\mu f$, for any function f. A valid gauge fixing condition, picks exactly one representative of these solutions. In the case of Lorentz gauge $\partial_\mu A^\mu = 0$, the e.o.m. reduces to the Klein-Gordon equation for every component of the wave function. The Lagrangian of a massless spin-1 particle is given by

$$\mathcal{L} = -\frac{1}{4}F^{\mu\nu}F_{\mu\nu} = \frac{1}{2}A_\mu\left(\partial^2 g^{\mu\nu} - \partial^\mu\partial^\nu\right) A_\nu + \text{boundary term} \tag{2.5}$$

where the field strength $F_{\mu\nu}$ is defined as $\partial_\mu A_\nu - \partial_\nu A_\mu$. The invariance of the theory to gauge transformations becomes evident in the formulation in terms of the field strength tensor, since itself is invariant. Gauge freedom prevents us from including a mass term $\propto A^2$, since such a combination is not gauge invariant. The Stueckelberg trick [7] allows for such a mass term, but it does not form part of the Standard Model of particle physics.

Fermion-Boson interactions

By promoting the global symmetry of the fermion field to a local one

$$\psi(x) \to e^{-i\alpha(x)}\psi(x), \tag{2.6}$$

and using a gauge transformation of the boson field with the same space-time function $f = \frac{1}{e}\alpha(x)$, one can form a gauge invariant Lagrangian by adding the interaction term

$$\mathcal{L}_{int} = -ej_\mu A^\mu \tag{2.7}$$

to the free fermion and boson Lagrangians. j_μ denotes the conserved current of the fermion Lagrangian. The interacting system can be written in terms of a covariant derivative, defined as

$$D_\mu = \partial_\mu + ieA_\mu. \tag{2.8}$$

Thus, yielding a compact formulation of the quantum electrodynamics Lagrangian:

$$\mathcal{L}_{QED} = \overline{\psi}(i\not{D} - m)\psi - \frac{1}{4}F^{\mu\nu}F_{\mu\nu}. \tag{2.9}$$

The interaction of fermions and bosons is therefore dictated by gauge transformations.

Quantization

Having set up the classical theory, the next step is to quantize it. The basic quantity of a free theory is the 2-point correlation function in the Feynman prescription. It is a Green function of the e.o.m., also called Feynman propagator, describing the propagation amplitude of the field between two space-time points. For a free fermion field with mass m it is given by

$$S_F(x-y) = \int \frac{d^4p}{(2\pi)^4} \frac{i(\not{p}+m)}{p^2 - m^2 + i\varepsilon} e^{-ip(x-y)}. \tag{2.10}$$

Where x and y denote the space-time points and p the momentum of the propagating field. The momentum is not constrained by the mass shell condition $p^2 = m^2$, which means that the field is allowed to be off-shell. For the boson propagator, difficulties are introduced by gauge invariance. This is most easily dealt within functional integral formulation of quantum field theory, for which I refer to [5]. Effectively one adds the gauge fixing term $\frac{-2}{\xi}(\partial_\mu A^\mu)^2$, due to the Faddeev-Popov procedure, to the Lagrangian which alters the boson correlation functions. The boson propagator depends on the unphysical parameter ξ, and is given by

$$D_F(x-y) = \int \frac{d^4p}{(2\pi)^4} \frac{-i}{p^2 + i\varepsilon}\left(g^{\mu\nu} - (1-\xi)\frac{p^\mu p^\nu}{p^2}\right) e^{-ip(x-y)}. \tag{2.11}$$

Where $g^{\mu\nu}$ denotes the space-time metric and the other variables are defined as in Eq. 2.10. The Faddeev-Popov method guarantees independence of the introduced parameter ξ, when computing physical observables. It is customary to pick a specific gauge, to shorten computations. Convenient choices are:

$$\xi = \begin{cases} 0 & \text{Landau gauge} \\ 1 & \text{Feynman gauge} \end{cases} \tag{2.12}$$

To obtain n-point correlation functions of a field ϕ between space-time points $x_1, x_2, \ldots x_n$, denoted as $\langle\Omega| T\phi(x_1)\phi(x_2)...\phi(x_n) |\Omega\rangle$, one takes functional derivatives of the theory's generating functional $Z[J]$. The generating functional is defined as

$$Z[J] = \int \mathcal{D}\phi \, e^{i\int d^4x[\mathcal{L}+J(x)\phi(x)]}, \tag{2.13}$$

where $J(x)$ represents an external classical source and the integration is performed over all classical field configurations, denoted as $\int \mathcal{D}\phi$. The n-point correlation functions are obtained by

$$\langle\Omega| T\phi(x_1)...\phi(x_n) |\Omega\rangle = \frac{1}{Z[J=0]}\Big(\frac{1}{i}\frac{\delta}{\delta J(x_1)}\Big)...\Big(\frac{1}{i}\frac{\delta}{\delta J(x_2)}\Big)Z[J]\Big|_{J=0}. \tag{2.14}$$

This yields sums of products of Feynman propagators for a free theory. For interacting theories, the exponential of the interacting Lagrangian is expanded in a Taylor series in the coupling, giving a perturbative expansion valid for small couplings. To obtain matrix elements from the correlation functions, the LSZ reduction formula is put into use:

$$\begin{aligned}&\langle p_3...p_n| 1 + iT |p_1p_2\rangle = \\ &\big[i\int dx_1^4 e^{-ip_1x_1}(\partial_1^2+m^2)\big]...\big[i\int dx_n^4 e^{ip_nx_n}(\partial_n^2+m^2)\big] \langle\Omega| T\phi(x_1)\phi(x_2)...\phi(x_n) |\Omega\rangle\,.\end{aligned} \tag{2.15}$$

Since 4-momentum is conserved in every process, this factor is extracted to define the matrix element $\mathcal{M}$:

$$\langle p_3...p_n| iT |p_1p_2\rangle = (2\pi)^4\delta^{(4)}\Big(\sum_{i=1,2} p_i - \sum_{i=3...n} p_i\Big)\, i\mathcal{M}. \tag{2.16}$$

It is the analogue of the quantum mechanical scattering amplitude f. $\mathcal{M}$ is the amplitude for the process to occur and can be related to observable quantities such as cross sections. A detailed calculation is performed in the appendix.
Richard Feynman invented a pictorial representation to derive the amplitude $\mathcal{M}$ via a simple set of rules:

$$i\mathcal{M} = \text{sum of all connected, amputated diagrams.} \tag{2.17}$$

Where further momentum conservation has to be imposed on each vertex and each undetermined loop momentum needs to be integrated (and an additional factor of (-1) for fermion loops), and if necessary, a division by the symmetry factor of the diagram needs to be included. The Feynman rules for field propagation and interaction in QED are given by

$$= \frac{-i}{p^2+i\varepsilon}\Big(g^{\mu\nu} - (1-\xi)\frac{p^\mu p^\nu}{p^2}\Big)$$

$$= \frac{i(\not{p}+m)}{p^2-m^2+i\varepsilon}$$

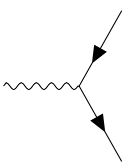

$$= -ie\gamma^\mu$$

where the solid (wavy) line represents fermions (bosons). As mentioned below Eq. 2.2, electrical charge is conserved in QED. This conservation is depicted with arrows denoting the flow of electrical charge. The rules for incoming (outgoing) particles of an interaction, denoted as a small circle, are given here on the left (right):

Fermions:	 $= u(p)$	 $= \bar{u}(p)$
Antifermions:	 $= \bar{v}(p)$	 $= v(p)$
Photons:	 $= \epsilon_\mu(p)$	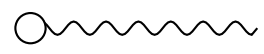 $= \epsilon^*_\mu(p)$

Antifermions are oppositely charged as fermions, which are again denoted by the charge flow arrows. Incoming and outgoing particles are on-shell and contribute solutions of their e.o.m. (in momentum space) to a diagram. For external fermions (antifermions) these are given by $u(p)$ ($v(p)$) spinors and for photons by the polarisation vector $\epsilon_\mu(p)$. The transversely polarized polarisation vector accounts for the two physical states of photons.
Computing higher order contributions (diagrams with loops) leads to divergent integrals. Changing the dimension of the integrals to $d = 4 - 2\epsilon$, for small ϵ, gives formally finite integrals which scale as inverse powers of ϵ. This is dimensional regularization, which is often used since it does not brake gauge invariance. In this context, an expression is said to be infinite, if it blows up in the limit $\epsilon \to 0$. The higher order contributions depend then on ϵ and μ, where the latter is an energy scale that ensures the scale dimension of the integral.

By the fact that higher order contributions are infinite, one concludes that the parameters in the Lagrangian itself are unphysical. In the framework of renormalized perturbation theory, the original ('bare') quantities in the Lagrangian are explicitly denoted by a 0 subscript:

$$\mathcal{L}_{QED} = \bar{\psi}_0(i\partial\!\!\!/)\psi_0 - \frac{1}{4}F_0^{\mu\nu}F_{\mu\nu\,0} - e_0\bar{\psi}_0\gamma_\mu\psi_0 A_0^\mu \tag{2.18}$$

(For what follows it suffices to consider massless QED). Realizing that higher order 2-point functions of the bare fields are infinite, one proceeds by defining renormalized fields, denoted with a R subscript, by

$$\psi_0 = Z_2^{1/2}\psi_R \quad \text{and} \quad A_0^\mu = Z_3^{1/2}A_R^\mu. \tag{2.19}$$

The ψ's are Dirac spinors and the renormalized fermion field ψ_R is not to be confused with the right-handed 2-component Weyl spinor. $Z_{2/3}$ are power series in the coupling constant containing higher order contributions to the 2-point functions. This field rescaling leads to

$$\mathcal{L}_{QED} = Z_2\bar{\psi}_R(i\partial\!\!\!/)\psi_R - Z_3\frac{1}{4}F_R^{\mu\nu}F_{\mu\nu\,R} - Z_1 e_R\bar{\psi}_R\gamma^\mu\psi_R A_{\mu\,R}, \tag{2.20}$$

where in the last term a renormalized charge e_R was defined by

$$Z_1 e_R = Z_2 Z_3^{1/2} e_0 \mu^{\frac{d-4}{2}}. \tag{2.21}$$

The power of μ ensures that e_R is dimensionless. By expanding $Z_X = 1 + \delta_X$ for $X \in \{1,2,3\}$, where δ_X is proportional to e_R^2, one obtains the Lagrangian of renormalized perturbation theory at 1-loop level:

$$\begin{aligned} \mathcal{L}_{QED} =& \overline{\psi}_R(i\partial\!\!\!/)\psi_R - \frac{1}{4}F_R^{\mu\nu}F_{\mu\nu\,R} - e_R\overline{\psi}_R\gamma^\mu\psi_R A_{\mu\,R} \\ &+ \delta_2\overline{\psi}_R(i\partial\!\!\!/)\psi_R - \delta_3\frac{1}{4}F_R^{\mu\nu}F_{\mu\nu\,R} - e_R\delta_1\overline{\psi}_R\gamma^\mu\psi_R A_{\mu R}. \end{aligned} \tag{2.22}$$

The additional terms, called counterterms, yield additional Feynman rules, which need to be included in higher order computations. For example the loop contribution of the photon self-energy, where the infinity is contained in $\Pi_2(p^2)$, is given by

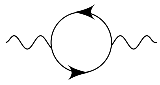

$$= -i(p^2 g^{\mu\nu} - p^\nu p^\mu)e_R^2\Pi_2(p^2). \tag{2.23}$$

The corresponding counterterm, given by the renormalized Lagrangian is given by

$$= -i(p^2 g^{\mu\nu} - p^\nu p^\mu)\delta_3. \tag{2.24}$$

Therefore, the one-particle irreducible (1PI) contribution up to order e_R^2 is given by

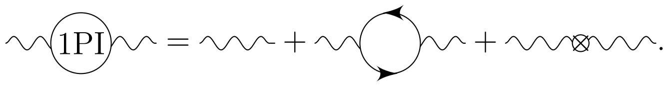

(2.25)

The photon propagator is obtained by the sum of all 1PI graphs. This summation forms a geometric series, which gives

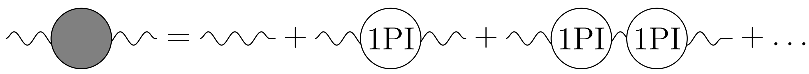

(2.26)

$$= -i\left(g^{\mu\nu} - \frac{p^\mu p^\nu}{p^2}\right)\frac{1}{p^2(1 + e_R^2\Pi_2(p^2) + \delta_3) + i\epsilon}. \tag{2.27}$$

By using renormalization conditions one defines the δ_X's, such that the renormalized n-point function are independent of ϵ and thus finite. For example, the on-shell renormalization condition for the photon self-energy fixes its residue of the pole at $p = 0$ to 1 via:

$$\delta_3 = -e_R^2\Pi_2(0) = -\frac{e_R^2}{12\pi^2}\frac{1}{\epsilon} - \frac{e_R^2}{12\pi^2}\ln\frac{\mu^2}{m_R}. \tag{2.28}$$

Where in the last line the result has been stated, which is derived in Appendix A. Since the terms δ_1 and δ_2 are not relevant for the following discussion, their expressions are not stated. Calculating n-point functions in renormalized perturbation theory then yields results independent of ϵ and μ. A somewhat easier scheme is minimal subtraction, in which only inverse powers of ϵ are absorbed in the counterterms, thus yielding $\delta_3 = -\frac{e_R^2}{12\pi^2}\frac{1}{\epsilon}$. The consequence is that higher order contributions still depend on the low energy scale μ, which parametrizes the renormalization. But by evaluating μ at a given scale of the diagram (electron mass in case of the photon

self-energy) one obtains the same result as before.
Renormalized perturbation theory further allows for a systematic study of the energy dependence of the renormalized (physical) coupling. This is done by observing that the bare charge does not depend on the renormalization scheme:

$$\mu \frac{d}{d\mu} e_0 = 0. \tag{2.29}$$

By using Eq. 2.21 one obtains an expression for the bar charge, given by

$$e_0 = e_R(1 + \delta_1 - \delta_2 - \frac{1}{2}\delta_3)\mu^\epsilon, \tag{2.30}$$

with the δ's introduced below Eq. 2.21. Inserting this expression in Eq. 2.29 yields a differential equation for e_R, the renormalization group equation. It is common to define

$$\beta(e_R) \stackrel{\text{def}}{=} \mu \frac{d}{d\mu} e_R. \tag{2.31}$$

The β function, a power series in the coupling, signifies the rate of coupling strength growth by increasing energy. For the special case of quantum electrodynamics $\delta_1 = \delta_2$, so only the photon self-energy counterterm δ_3 is responsible for the running of the coupling. The renormalization group equation leads to $\beta = -\epsilon e_R + \frac{e_R^3}{12\pi^2}$. The limit $\epsilon \to 0$ is well defined and does not depend on the subtraction scheme. The positive β function in QED tells us that the coupling grows stronger at higher energies.

2.1.2. Yang-Mills theory

Quantum electrodynamics is a special case of the more general Yang-Mills theory. Gauge transformations, as space-time transformations, form a group. The gauge group of quantum electrodynamics is the abelian group $U(1)$, corresponding to the invariance under phase transformations in Eq. 2.6. Yang and Mills extended this formalism to non-abelian gauge groups, which means that the generators of the symmetry t^a do not commute $[t^a, t^b] = i f^{abc} t^c$, where f^{abc} are the structure constants of the gauge group.
In Yang-Mills theory, fermion fields form an n-plet ψ_i, where each i denotes a Dirac spinor. This multiplet transforms with an $n \times n$ unitary matrix under local gauge transformations. The covariant derivative is altered to

$$(D_\mu \psi)_i = (\partial_\mu \delta_{ij} - ig A_\mu^a t_{ij}^a)\psi_j, \tag{2.32}$$

incorporating one gauge field A_μ^a, with index a, for every generator of the gauge group. The number of independent generators depends on the gauge group, for the most interesting $SU(n)$ it is $n^2 - 1$. Furthermore, we get as many field strength tensors as gauge fields, which are defined as

$$F_{\mu\nu}^a = \partial_\mu A_\nu^a - \partial_\nu A_\mu^a + g f^{abc} A_\mu^b A_\nu^c. \tag{2.33}$$

As opposed to quantum electrodynamics, these quantities are not invariant under gauge transformations. The Lagrangian of Yang-Mills theory appears to be the same as Eq. 2.9, with explicit inclusion of the additional indices it reads

$$\mathcal{L}_{YM} = i\bar{\psi}_i(\not{D}\psi)_i - m\bar{\psi}_i\psi_i - \frac{1}{4}F^{a\,\mu\nu}F^a_{\mu\nu}, \tag{2.34}$$

where a sum over the repeated index i (a), accounting for fermion fields in the n-plet (generators of the gauge group), is implied. An important difference to quantum electrodynamics is the non-linear e.o.m. of non-abelian gauge theories. This feature gives self interacting gauge boson vertices. The Lagrangian is invariant under the following infinitesimal gauge transformation

$$\psi_i \to (\delta_{ij} + i\alpha^a t^a_{ij})\psi_j \quad \text{and} \quad A^a_\mu \to A^a_\mu + \frac{1}{g}\partial_\mu\alpha^a + f^{abc}A^b_\mu\alpha^c, \tag{2.35}$$

with an arbitrary function $\alpha^a(x)$ for every index a. A complication arises in quantization of non-abelian gauge theories. To consistently perform the quantization one needs to include so called ghost fields, which cancel unphysical polarisations of gauge bosons. These ghosts, as the name suggests, are not physical observables but ensure the unitarity of the theory. So the final ingredient to non-abelian gauge theories is the following ghost term, which follows from functional quantization

$$\mathcal{L}_{ghost} = \bar{c}^a(-\partial^2\delta^{ac} - g\partial^\mu f^{abc}A^b_\mu)c^c. \tag{2.36}$$

The β function, defined for QED in Eq. 2.31, of non-abelian gauge theories depends, unlike quantum electrodynamics, on all counterterms. For a $SU(N)$ gauge theory with n_f fermions transforming in the fundamental representation it is given by:

$$\beta(g) = -\left(\frac{11}{3}N - \frac{2}{3}n_f\right)\frac{g^3}{(4\pi)^2}. \tag{2.37}$$

2.2. The Standard model of particle physics

The previous section introduced the basic ingredients for a successful description of elementary particle physics, except electroweak symmetry breaking. The Standard model of particle physics is a quantum field theory with gauge group $SU(3)_C \times SU(2)_L \times U(1)_Y$, where $SU(2)_L \times U(1)_Y$ is the gauge group of electroweak interactions, which incorporates quantum electrodynamics. Electroweak theory will be the topic of the next section, which further introduces the concept of spontaneous symmetry breaking (SSB). After SSB the residual gauge group of the Standard Model is $SU(3)_C \times U(1)_{em}$. This section concludes with quantum chromodynamics, the theory of strong interactions with gauge group $SU(3)_C$. Fig. 2.1 displays the particle content of the Standard Model, which is now introduced.

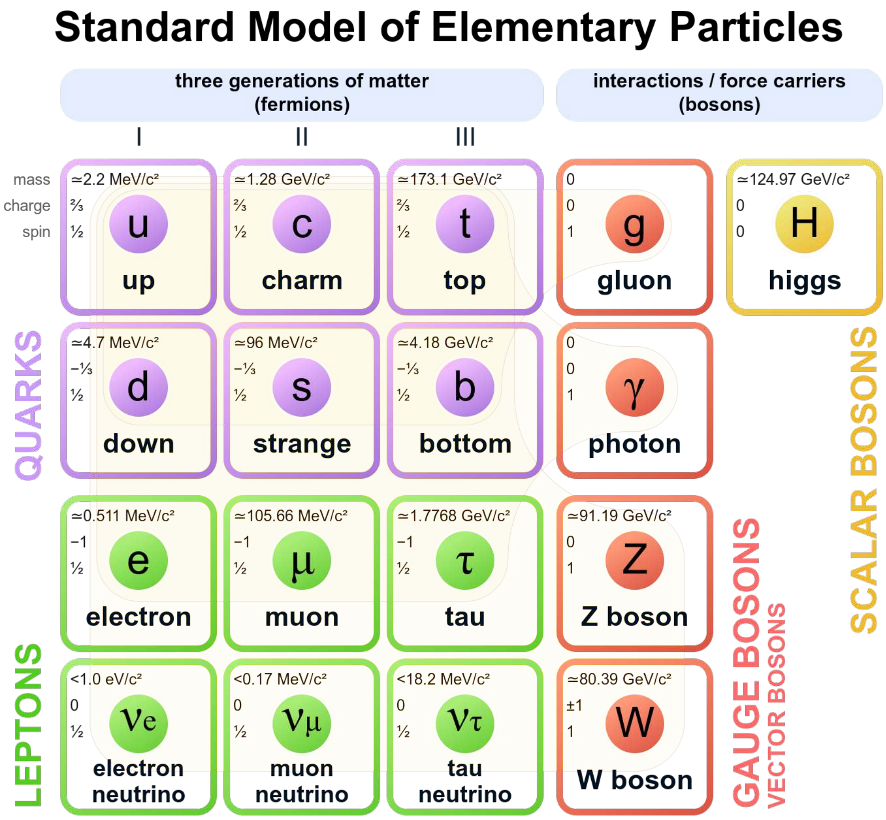

Figure 2.1.: Particle content of the Standard Model of particle physics. From [8].

Table 2.1.: Fermion content of the Standard Model of particle physics.

	1^{st} Gen.	2^{nd} Gen.	3^{rd} Gen.	$SU(3)_C \times SU(2)_L \times U(1)_Y$
l_L^i	$\begin{pmatrix} \nu_e \\ e^- \end{pmatrix}_L$	$\begin{pmatrix} \nu_\mu \\ \mu^- \end{pmatrix}_L$	$\begin{pmatrix} \nu_\tau \\ \tau^- \end{pmatrix}_L$	($\mathbf{1}$,$\mathbf{2}$,-1/2)
e_R^i	e_R^-	μ_R^-	τ_R^-	($\mathbf{1}$,$\mathbf{1}$,-1)
q_L^i	$\begin{pmatrix} u \\ d \end{pmatrix}_L$	$\begin{pmatrix} c \\ s \end{pmatrix}_L$	$\begin{pmatrix} t \\ b \end{pmatrix}_L$	($\mathbf{3}$,$\mathbf{2}$,1/6)
u_R^i	u_R	c_R	t_R	($\mathbf{3}$,$\mathbf{1}$,2/3)
d_R^i	d_R	s_R	b_R	($\mathbf{3}$,$\mathbf{1}$,-1/3)

2.2.1. Electroweak theory $SU(2)_L \times U(1)_Y$

The theory of electroweak interactions is a chiral theory, meaning that left and right handed spinor components couple differently to gauge bosons. The covariant derivative, encoding the interactions, is given by

$$D_\mu = \mathbb{1}\partial_\mu - igA_\mu^a \frac{\sigma^a}{2} - i\mathbb{1}g'YB_\mu. \tag{2.38}$$

Where g, A_μ^a (g', B_μ) are the coupling and gauge bosons of the gauge group $SU(2)$ $\big(U(1)\big)$. $\frac{\sigma^a}{2}$ are the generators of the $SU(2)$ gauge group, and σ^a denote the Pauli matrices. Y is the hypercharge, which depends on the field on which the derivative acts. The covariant derivative acts on fermion fields in multiplets: Left handed particles are grouped in doublets, whereas right handed ones transform as singlets. Table 2.1 lists the fermion content of the Standard Model. The last column states the transformation properties: The $SU(2)$ value defines if it is a doublet ($\mathbf{2}$) or singlet ($\mathbf{1}$), and the $U(1)_Y$ value is the hypercharge for the field.

As discussed in section 2.1.1, it is not possible to include boson masses in gauge theories. Furthermore, no gauge invariant mass terms ($\propto \overline{\psi}_R\psi_L + \overline{\psi}_L\psi_R$) for fermions can be formed, since left and right handed particles belong to different representations of the gauge group. But the mechanism of spontaneous symmetry breaking furnishes a way to include mass terms for both cases. For this purpose a complex scalar field H, transforming as a doublet in $SU(2)_L$ with hypercharge $Y = \frac{1}{2}$, is added to the Lagrangian:

$$\mathcal{L}_{SSB} = (D^\mu H)^\dagger (D_\mu H) - V(H), \quad V(H) = -\mu^2 H^\dagger H + \lambda (H^\dagger H)^2, \quad \text{where } \mu^2 > 0. \tag{2.39}$$

The potential V has a mexican hat shape, whose minimum is at $(H^\dagger H) = \left(\frac{\mu^2}{2\lambda}\right) = \frac{v^2}{2}$. This collection of preferred states breaks the symmetry of the Lagrangian. Specifically, three transformations are broken and one remains intact. The field H can be expanded around this minimum and written in terms of real fields as

$$H = \frac{1}{\sqrt{2}} \begin{pmatrix} -i(\phi_1 - i\phi_2) \\ v + (h + i\phi_3) \end{pmatrix}. \tag{2.40}$$

At this point it is advisable to use unitary gauge, in which the Goldstone bosons ϕ_i are absent. The remaining excitation along the direction of the unbroken symmetry h, the Higgs field, acquires a mass given by $m_h = \sqrt{2\lambda}v$. This is seen by expanding the potential term $V(H)$ around the minimum. Furthermore, it gives self interacting terms $\propto h^3$ and h^4. The kinetical term of the Lagrangian $(D^\mu H)^\dagger(D_\mu H)$, contains the gauge bosons in the covariant derivative and yields a mass term for the bosons associated with the broken symmetries. This is Goldstone's theorem. Furthermore, the kinetical term has interacting terms of the Higgs field and the massive gauge bosons. Rotating to the mass eigenstates of the gauge bosons (Z and W boson), the covariant derivative reads

$$\begin{aligned} D_\mu &= \partial_\mu - i\frac{g}{\sqrt{2}}(W_\mu^+ T^+ + W_\mu^- T^-) - i\frac{g}{\cos\Theta_w} Z_\mu (T^3 - \sin^2\Theta_w Q) - ieA_\mu Q \\ T^\pm &= \frac{1}{2}(\sigma^1 \pm \sigma^2) \end{aligned} \tag{2.41}$$

The rotation angle, the Weinberg angle, is given by $\cos\Theta_w = \frac{g}{\sqrt{g^2+g'^2}}$. It further relates the masses of the gauge bosons W and Z via $m_W = g\frac{v}{2} = m_Z\cos\Theta_w$. The last part of Eq. 2.41 is the familiar quantum electrodynamics interaction with the massless photon A_μ. The charge Q is given by $Q = T^3 + Y$. The number T^3 depends on the field the covariant interaction acts on, it is 0 for singlets and $\pm 1/2$ for doublets (plus for the upper entry of the doublet).
Using these doublets, singlets and the scalar field H we can also introduce gauge invariant mass terms for fermions. For example for the leptons of the 1^{st} generation it reads:

$$\mathcal{L}_{\text{Yukawa}} = -\lambda_e^1\, \overline{l_L^i} \cdot He_R^1 + h.c = -\frac{v}{\sqrt{2}}\lambda_e^1 \overline{e^-}_L e_R^- + h.c. \tag{2.42}$$

where the vacuum expectation of H has been inserted. Thus yielding a mass term $m_e = \frac{1}{\sqrt{2}}\lambda_e^1 v$. The vacuum expectation value of the scalar field is given by $v = 246$ GeV, and λ_e^1 is the Yukawa coupling of the electron. The expectation value of the scalar field is determined by the knowledge of g and m_W in $m_W = g\frac{v}{2}$. The discovery of the Higgs boson fixed its mass m_h and allows for determination of the parameters in the Higgs potential. Furthermore, measuring the Higgs self-coupling is a primary goal for future colliders.

2.2.2. Quantum chromodynamics $SU(3)_C$

In table 2.1 the fermions of the Standard Model of particle physics are listed. One type of particles, quarks, cannot be observed directly. They are the subject of quantum chromodynamics (QCD), a Yang-Mills theory with gauge group $SU(3)_C$. The gauge bosons, which the theory has eight, are called gluons. As discussed in the previous section, fermions come in multiplets in this theory. In quantum chromodynamics the entries of a multiplet are referred to as three different colors, hence the name. An important feature of quantum chromodynamics is asymptotic freedom,

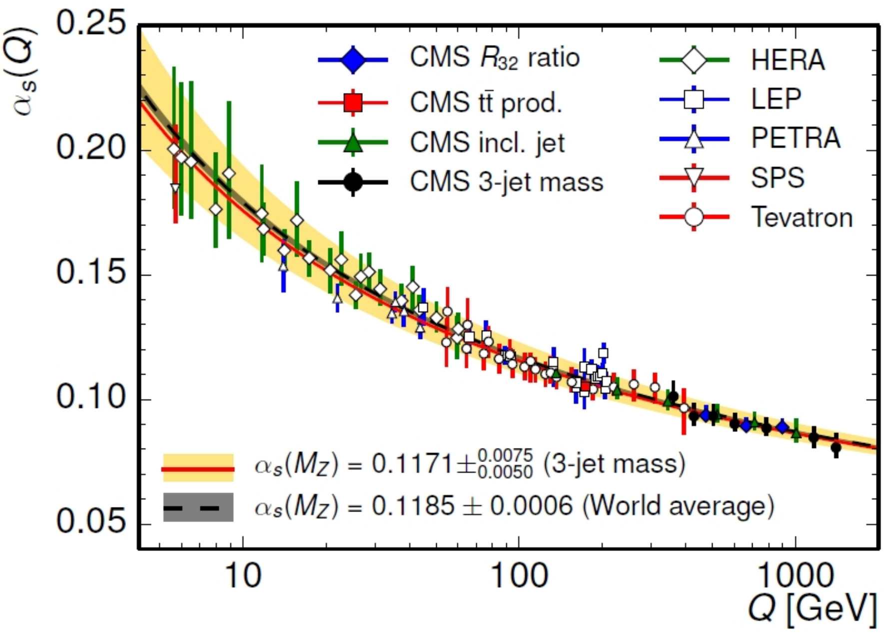

Figure 2.2.: Measurement of α_s at various energy scales. From [9].

which means that the gauge coupling, denoting the interaction strength between colored states, decreases with increasing energy. Consider Fig. 2.2 for measurements of the strong coupling constant at different energy scales. The running of the coupling is predicted by the negative β function of QCD. Evaluating Eq. 2.37 for QCD ($N = 3$ and $n_f = 6$) gives the β function for QCD:

$$\beta(g_s) = -7\frac{g_s^3}{(4\pi)^2}. \tag{2.43}$$

The low coupling at high energies allows for a perturbative description of scattering events at hadron colliders. For low energies, the coupling is high and the perturbative expansion brakes down. As mentioned at the beginning of this section, quarks are not directly observable. Only colorless states, such as baryons (mesons) consisting of three quarks or antiquarks (a quark and a antiquark) are observable. This is called color confinement of QCD.

2.3. Issues with the Standard Model of particle physics

Although the Standard Model of particle physics provides a very successful description of elementary particles, there are still unsolved problems and discrepancies. Evidences for these issues come from two complementary sources. Firstly, from high precision measurements at colliders where the smallest structures of matter are resolved. And secondly, from cosmological observations which deal with the biggest scales in our universe.

The Standard Model of Cosmology is the ΛCDM Model. Λ stands for dark energy which drives the accelerated expansion of our universe. Observations of rotation curves of galaxies furthermore indicate a large amount of invisible matter. This is also deduced from rotational velocities of galaxy clusters (first done by Zwicky in 1933 [10]). Another hint of gravitationally interacting invisible matter comes from gravitational lensing [11]. The matter distribution of objects causing gravitational lensing is deduced, and shown to be different from their distribution of luminous matter. Based on its invisibility it is referred to as dark matter. The Standard Model of Cosmology includes cold dark matter CDM, which means that its velocity is very small compared to the speed of light. It is the most prominent model for dark matter. Furthermore, dark matter plays an important part in structure formation of our universe. Without it, the universe would still be homogeneous and would not have formed the structure we observe. Lastly, the anisotropies of the cosmic microwave background, most accurately measured by the Planck collaboration, provides information on the content of the universe. These data are fitted to the ΛCDM model, yielding a dark matter content of the universe of about 26% and a dark energy content of about 69% [12]. The Standard Model of particle physics has no explanation for dark matter, although many attempts have been made to explain it within the Standard Model, or ideas for extensions to explain it [11]. Another open problem is the matter-antimatter asymmetry. There is no explanation why we are surrounded by matter but only little antimatter. So the question arises how this asymmetry has been produced.

The anomalous magnetic moment of the muon is one example of an inconsistency in the Standard Model from precision measurements. The current theoretical calculations and measurements [13] deviate at 3σ level from the Standard Model. The follow up experiment is currently performed at the Brookhaven National Laboratory and results are expected in the course of 2020. Another example are decays of B mesons, which indicate deviations from the Standard Model of particle physics [14]. The publication discusses hints for a possible lepton flavor violation in B decays, observed by LHCb and Belle. Another puzzle concerns neutrinos: in the Standard model of particle physics neutrinos are massless. Observations show neutrino oscillations, which requires mass. It is possible to add a right handed neutrino to the Standard Model to introduce neutrino masses, but such a neutrino has not been observed so far.

3. Leptophilic flavor non-universal Z'

In the previous chapter the Standard Model of particle physics (SM) was introduced. The chapter concluded with shortcomings of the theory which motivates for searches beyond the Standard Model (BSM). One of the simplest extensions to the SM is an additional $U(1)$ gauge symmetry, mediated by an additional gauge boson. Such extensions are usually referred to as Z' models in which the massive mediator is colorless, and therefore does not form part of QCD. Furthermore, Z' bosons are electrically neutral as the Z boson of the SM, hence the name. In what follows a leptophilic Z' model is studied. In these models the Z' gauge boson interacts at leading order only with leptons of the SM particle spectrum. More specifically, couplings only to electrons, muons and their neutrinos are assumed. Such a gauge extension is given e.g. by the $L_e - L_\mu$ model. In this model the new gauge boson couples with opposite charge to the two involved lepton flavors. In this thesis a simplified model is assumed with generic couplings to electrons and muons. In the next section, the model, which was proposed in the context of dark matter searches [3], is introduced. Furthermore, interference effects with the SM are presented. Searches for leptophilic Z' bosons at the LHC are discussed and the, for this thesis relevant Drell-Yan process at the LHC. Finally, exclusion limits from other experiments constraining the studied leptophilic Z' model are presented.

3.1. Theory

In [3] the massive Z' boson is introduced via a simplified model. The Lagrangian of the Standard Model is altered by an interaction part between Z' and known Standard Model particles. The origin of the mass for the new boson is not specified. Either it comes from a spontaneous symmetry breaking mechanism or new degrees of freedom are required to UV complete the simplified model at high energies. A simplified model approach needs to be contrasted with the also very popular effective field theory (EFT) approach. In the latter new massive mediators are integrated out at a scale Λ and thus are absent in the effective description. This procedure produces non-renormalizeable contact operators in the Lagrangian. An example is Fermi theory of weak interactions and also the limits from LEP for the Z' model, which are discussed in section 3.5. In an EFT, cross section calculations lead to contributions growing with energy transfer $\frac{\hat{s}}{\Lambda^2}$. This approach is applicable if the momentum transfer is small compared to the cut-off scale, e.g. the mass of the vector boson which was integrated out. But at higher energies unitarity is violated, see [15] for a detailed discussion. Therefore, the EFT approach allows studying deviations from SM, but no direct searches for massive vector bosons. In the context of simplified models, the mediator stays in the theory, thus allows for resonance searches. The simplified model interaction Lagrangian, proposed in [3], is given by

$$\mathcal{L}_{int} = (J_\mu^{(\text{charged leptons})} + J_\mu^{(\text{neutrinos})})Z'^\mu, \tag{3.1}$$

where the currents are separated in charged leptons and neutrinos:

$$J_\mu^{(\text{charged leptons})} = \sum_{l=e,\mu} \bar{l}\gamma_\mu(g_{Vl} + g_{Al}\gamma^5)l \tag{3.2}$$

$$J_\mu^{(\text{neutrinos})} = \sum_{l=e,\mu} (g_{Vl} - g_{Al})\bar{\nu}_l\gamma_\mu\Big(\frac{1-\gamma^5}{2}\Big)\nu_l. \tag{3.3}$$

The coupling structure to neutrinos is dictated by the requirement of gauge invariance which means that left handed particles of an SU(2) doublet are required to have the same coupling. No right handed neutrinos are added to the Standard Model particle content. The vector- and axial vector couplings $g_{V/A}$ in Eq. 3.2 are specified at a large scale Λ_{UV}. In what follows $\Lambda_{\text{UV}} = 10$ TeV is assumed. The renormalization group equation (RGE) allows for studying this couplings at a low energy scale μ. The procedure is most clearly outlined in [16]. The coupling of the Z' boson to fermions can be matched to the operator

$$c_i Z'^\mu \overline{\psi_i}\gamma_\mu\psi_i, \tag{3.4}$$

where ψ_i is one of the 15 SM fermion fields ($l_L^j, e_R^j, q_L^j, u_R^j, d_R^j$ for every generation $j \in 1,2,3$) with specified hypercharge listed in Tab. 2.1. This matching yields c_i at scale Λ_{UV}, since $g_{V,A}$ are defined at this scale. Actually, it suffices to consider 5 SM fields, since the induced coupling is generation independent. But since the Z' model is flavor dependent, one avoids confusion by considering all 15 SM fields. For example, for the left handed electron flavored $SU(2)$ doublet $l_L^1 = (\nu_e\ e)_L^T$ Eq. 3.4 reads

$$c_{l_L^1} Z'^\mu \overline{l_L^1}\gamma_\mu l_L^1 = c_{l_L^1} Z'^\mu(\overline{\nu_{eL}}\gamma_\mu\nu_{eL} + \overline{e_L}\gamma_\mu e_L). \tag{3.5}$$

Here, the aforementioned requirement for the neutrinos to have the same coupling as the charged lepton is explicit. Similarly, for the right handed electron $e_R^1 = e_R$ it reads

$$c_{e_R^1} Z'^\mu \overline{e_R^1}\gamma_\mu e_R^1 = c_{e_R^1} Z'^\mu \overline{e_R}\gamma_\mu e_R. \tag{3.6}$$

Comparing the simplified model in Eq. 3.1 to Eq. 3.6 yields the matching for the electron

$$Z'^\mu(c_{l_L^1}\overline{e_L}\gamma_\mu e_L + c_{e_R^1}\overline{e_L}\gamma_\mu e_L) = Z'^\mu\, \bar{e}\gamma_\mu(g_{Ve} + g_{Ae}\gamma^5)e. \tag{3.7}$$

Using the projectors $P_{R/L} = \frac{1\pm\gamma^5}{2}$, one obtains the matching given by $g_{V,A\,e} = (\pm c_{l_L^1} + c_{e_R^1})/2$. Similarly, for the muon $g_{V,A\,\mu} = (\pm c_{l_L^2} + c_{e_R^2})/2$, where the 2 in the c's index refers to the 2^{nd} generation. The same applies for the matching of the quark couplings, but since the Z' model has no tree-level coupling to quarks the c's denoting Z' couplings to quarks are zero at scale Λ_{UV}. With the matched couplings $c_i(\Lambda_{UV})$, the next step is to perform the running of the c's to a lower scale μ. After obtaining the low energy couplings $c_i(\mu)$ the matching can be reversed to obtain the couplings $g_{V,A}(\mu)$ at the low energy scale μ. The running due to hypercharge interactions is driven by the following diagram

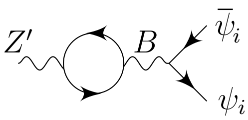

(3.8)

The loop contains particles with couplings to Z' and B, as charged leptons and neutrinos. The RGE yields the following coupling at energy scale μ:

$$c_i(\mu) = c_i(\Lambda_{UV}) + \frac{2}{3}\frac{\alpha_Y}{\pi} y_i \Big(\sum_{l \in e,\mu} g_{Vl} \Big) \ln \frac{\Lambda_{\mathrm{UV}}}{\mu} \tag{3.9}$$

where y_i is the hypercharge of the ψ field ($l_L^j, e_R^j, q_L^j, u_R^j, d_R^j$ for every generation $j \in 1, 2, 3$) listed in Table 2.1. For convenience, the hypercharges are restated here:

$$y_{l_L^j} = -1/2,\ y_{e_R^j} = -1,\ y_{q_L^j} = 1/6,\ y_{u_R^j} = 2/3,\ y_{d_R^j} = -1/3,\ \text{for } j \in \{1, 2, 3\}. \tag{3.10}$$

The hypercharge fine structure constant is defined by $\alpha_Y = g'^2/(4\pi)$. This result is derived in App. A. As mentioned above the induced coupling does not depend on the generation of the ψ field since the hypercharge is the same for all generations of one field. Inserting the hypercharges the induced couplings can be matched to vector and axial vector notation as discussed above. For quarks this matching is obtained by performing the same steps as for leptons. For up type quarks it is given by $g_{V,A\,u} = (\pm c_{q_L} + c_{u_R})/2$ and for down type quarks by $g_{V,A\,d} = (\pm c_{q_L} + c_{d_R})/2$. The induced couplings to up and down type quarks are given by

$$\{g_{Vu}(\mu), g_{Vd}(\mu), g_{Au}(\mu), g_{Ad}(\mu)\} = \Big\{ \frac{5}{18}, -\frac{1}{18}, \frac{1}{6}, -\frac{1}{6} \Big\} \frac{\alpha_Y}{\pi} \Big(\sum_{l \in e,\mu} g_{Vl} \Big) \ln \frac{\Lambda_{\mathrm{UV}}}{\mu} \tag{3.11}$$

Due to the different hypercharges of the SM fields one obtains different couplings to up and down type quarks. As discussed, these are generation independent since the hypercharges are the same for SM fields for all generations. The induced couplings to leptons also alter their tree-level couplings by

$$\{\Delta g_{Vl}(\mu), \Delta g_{Al}(\mu)\} = \Big\{ -\frac{1}{2}, -\frac{1}{6} \Big\} \frac{\alpha_Y}{\pi} \Big(\sum_{l \in e,\mu} g_{Vl} \Big) \ln \frac{\Lambda_{\mathrm{UV}}}{\mu}. \tag{3.12}$$

As above the induced coupling is generation independent and therefore also the alteration of the tree-level couplings, although their tree-level values may be different. At this point it is instructive to estimate the order of the induced couplings. Since the focus of this thesis is LHC phenomenology the scale of the induced coupling is evaluated at $\mu \approx 1$ TeV for this estimation. For performing the analysis, the scale μ will be evaluated at the mass of the Z' boson. The hypercharge coupling constant at the Z mass is given by $g' \approx 0.35$ [16], which yields

$$\alpha_Y = g'^2/(4\pi) = 9.7 \times 10^{-3} \approx 10^{-2}. \tag{3.13}$$

At $\mu \approx 1$ TeV the logarithmic term in Eq. 3.11 is $\ln \frac{\Lambda_{\mathrm{UV}}}{\mu} \approx 2.3$. Therefore, the induced couplings to quarks at $\mu \approx 1$ TeV are of the order of 10^{-3}. For completeness, the induced coupling of the Z' boson to the Higgs current $H^\dagger i \overleftrightarrow{D}_\mu H$ is also discussed. The term is given by $c_H Z'^\mu H^\dagger i \overleftrightarrow{D}_\mu H$. At tree-level no such coupling is given in the simplified model in Eq. 3.1, but hypercharge and Yukawa interactions induce it at loop level. The relevant diagrams are given by

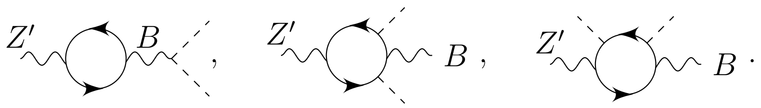

(3.14)

The first one has the same structure as the induced couplings to fermions, and the last two diagrams are due to Yukawa couplings. As discussed in App. A the Yukawa interactions are negligible compared to the hypercharge interactions, and are therefore neglected. Although not relevant, it is worth mentioning that the Yukawa corrections are proportional to the axial couplings g_{Al} of the fermions to the Z' boson [3]. Since the left diagram in Eq. 3.14 has the same structure as the induced couplings to fermions, the running is also given by Eq. 3.9 with $c_H(\Lambda_{UV}) = 0$. Inserting the hypercharge of the Higgs field ($Y = 1/2$) yields the running given by

$$c_H(\mu) = \frac{1}{3}\frac{\alpha_Y}{\pi}\Big(\sum_{l \in e,\mu} g_{Vl}\Big) \ln \frac{\Lambda_{\mathrm{UV}}}{\mu} \tag{3.15}$$

As discussed above, this yields a coupling of the order of 10^{-3} for $\mu \approx 1$ TeV. In App. C the decay width of the Z' boson is calculated. The partial decay width of the Z' boson to a pair of leptons is given by

$$\Gamma_{Z' \to \bar{l}l} = \frac{(g_V^l)^2 + (g_A^l)^2}{12\pi} m_{Z'}. \tag{3.16}$$

As mentioned at the beginning of this section the Z' boson needs to obtain its mass via a spontaneous symmetry breaking mechanism or new degrees of freedom are necessary to UV-complete this model. In the first case the Z' is a gauge boson of a hypothetical $U(1)'$ gauge symmetry, which is then broken to obtain the boson mass. A gauge symmetry needs to be anomaly free, otherwise unitarity is violated. Anomalous symmetries are symmetries of the classical field theory which are not respected in the quantum formulation. They are evaluated by calculating the contribution of triangle diagrams [5]. The SM is anomaly free for every generation of fermions, and forces electrical charges to be quantized. For additional gauge symmetries the triangle diagrams yield sets of equations for the new charges to be fulfilled to be anomaly free [17]. A leptophilic anomaly free $U(1)$ extension of the SM is e.g. given by the $L_e - L_\mu$ model. As above, only electrons and muons and their neutrinos couple to the gauge boson in the $L_e - L_\mu$ model. The couplings of this model, in the notation of the simplified model, are given by:

$$g_{Ve} = 1g' \quad g_{V\mu} = -1g', \tag{3.17}$$

where the number denotes the charge and g' the coupling constant of the $U(1)'$ gauge symmetry. Thus, we see that the anomaly free model does not induce couplings to quarks in this simplified model approach, since the sum of the couplings is zero, $\sum_{l \in e,\mu} g_{Vl} = 0$. Although not appealing, one can remove gauge anomalies by adding additional fermions to the theory [18]. If the new fermions do not couple to the hypercharge boson, the induced coupling does not change.

3.2. Interference effects

Apart from SM and the hypothetical leptophilic Z' contributions to the Drell-Yan process there are also interference effects between the two of them. It is best to understand their importance in the considered model at parton level. As derived in App. B, the cross section of a process with a massive vector boson in the s-channel is proportional to

$$\frac{\hat{s}}{(\hat{s} - m_i^2)^2 + m_i^2 \Gamma_i^2}. \tag{3.18}$$

where $\hat{s}$ denotes the partonic center of mass energy. It is given by $\hat{s} = (\hat{p}_1 + \hat{p}_2)^2$, where $\hat{p}_1$ and $\hat{p}_2$ denote the momentum of the colliding partons. Eq. 3.18 is the Breit-Wigner shape, which peaks at $\hat{s} = m_i^2$. The width of the peak is described by Γ. It denotes the width of the peak at half maximum. The same expression holds for massless bosons giving the expected $\propto 1/\hat{s}$. To study the interference between Z' and the SM it is best to analyse the kinematical contribution (depending on $\hat{s}, m, \Gamma$) and the coupling structure separately. To full generality we consider a generic interference term between two massive bosons denoted with subscript i and j. The kinematical term is given by

$$\frac{\left(\hat{s} - m_i^2\right)\left(\hat{s} - m_j^2\right) + \left(m_i \Gamma_i\right)\left(m_j \Gamma_j\right)}{\left[\left(\hat{s} - m_i^2\right)^2 + m_i^2 \Gamma_i^2\right]\left[\left(\hat{s} - m_j^2\right)^2 + m_j^2 \Gamma_j^2\right]}. \tag{3.19}$$

The denominator is strictly positive, but the first part of the numerator changes sign whenever $\hat{s}$ reaches the squared mass of an involved boson m^2. Furthermore, this part is zero at the resonance masses. Fig. 3.1 shows the region for constructive and destructive interference for the two interferences $Z - Z'$ and $\gamma - Z'$, following the kinematical term given by Eq. 3.19. Therefore, the peak of a resonance gets

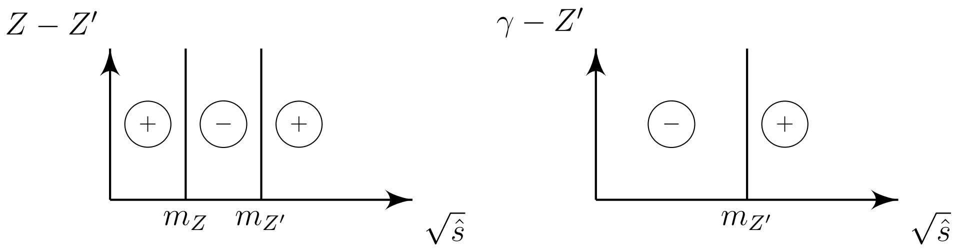

Figure 3.1.: Regions for constructive and destructive interference for the two interference terms $Z - Z'$ and $\gamma - Z'$, following the kinematical term given in Eq. 3.19.

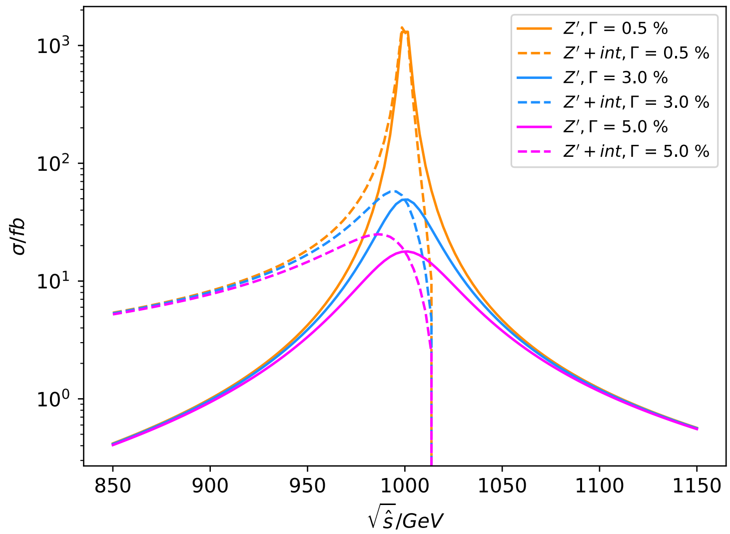

Figure 3.2.: Comparison of the Z' resonance peak with and without interference with Standard Model for a Z' mass of 1000 GeV.

shifted by interference effects. Fig. 3.2 compares the resonance shape, with and without interference with the Standard Model Z and γ, for a Z' mass of 1000 GeV and various Z' widths. The shift increases with the width of the new resonance. Furthermore, the contribution of Z' plus interference effects can also be negative, reducing the expected yields of the Standard Model Drell-Yan process. As derived in App. B the interference effect is, apart from the kinematical term discussed above, also proportional to the following coupling structure

$$(g^q_{Vi} g^q_{Vj} + g^q_{Ai} g^q_{Aj})(g^l_{Vi} g^l_{Vj} + g^l_{Ai} g^l_{Aj}), \tag{3.20}$$

where the first (second) bracket denotes the couplings of the interfering bosons, with subscript i and j, to the initial quarks (final leptons). Tab. 3.1 lists the couplings of the Standard Model γ and Z in g_V and g_A notation. As an example, consider the first bracket of Eq. 3.20 for $\gamma - Z'$ interference, with up type quarks as initial

	γ, e				Z, $\frac{e}{\sin\theta_w \cos\theta_w}$			
	g_V	g_A	g_L	g_R	g_V	g_A	g_L	g_R
ν_e, ν_μ, ν_τ	0	0	0	0	1/2	-1/2	1/2	0
e, μ, τ	-1	0	-1	-1	$\sin^2\theta_w$	-1/2	$-1/2 + \sin^2\theta_w$	$\sin^2\theta_w$
u, c, t	2/3	0	2/3	2/3	-2/3 $\sin^2\theta_w$	1/2	$1/2 - 2/3\sin^2\theta_w$	-2/3 $\sin^2\theta_w$
d, s, b	-1/3	0	-1/3	-1/3	1/3 $\sin^2\theta_w$	-1/2	$-1/2 + 1/3\sin^2\theta_w$	1/3 $\sin^2\theta_w$

Table 3.1.: γ, Z couplings in g_V, g_A notation. Common factors are stated in the header.

states. It reads

$$(g^{up}_{V\gamma} g^{up}_{VZ'} + g^{up}_{A\gamma} g^{up}_{AZ'}) = \Big((\frac{2}{3}e)(\frac{5}{18}k \sum_{l\in e,\mu} g_{Vl}) + (0e)(\frac{5}{18}k \sum_{l\in e,\mu} g_{Vl}) \Big) \tag{3.21}$$

where the induced couplings to up quarks from Eq. 3.11 has been inserted and k is defined as $k = \frac{\alpha_Y}{\pi} \ln \frac{\Lambda_{\text{UV}}}{\mu}$ to shorten the notation from the induced couplings. Note that k is strictly positive. The first (second) term denotes the contribution of vectorial (axial vectorial) couplings. Since the axial vector coupling of γ to quarks is zero, also the axial vector coupling of the Z' boson does not contribute. The overall contribution in Eq. 3.21 is positive for $\sum g_{Vl} > 0$. For $Z - Z'$ interference the axial vector coupling of the Z' boson to quarks does contribute because of the non-vanishing axial vector couplings of the Z boson to quarks. Performing this exercise also for down type quarks and $Z - Z'$ interferences yields the result that the first bracket of Eq. 3.20 is positive for both, $Z - Z'$ and $\gamma - Z'$ interference, if $\sum g_{Vl} > 0$. This is true for up and down type quarks. The second bracket in Eq. 3.20 depends on the vector g_V and axial-vector g_A coupling of the final state leptons l to the Z' boson. For $\gamma - Z'$ interference it is given by

$$(g^l_{V\gamma} g^l_{VZ'} + g^l_{A\gamma} g^l_{AZ'}) = \Big((-1e)(g_{Vl}) + (0e)(g_{Al}) \Big). \tag{3.22}$$

As above, the axial vector coupling of the Z' boson to leptons does not contribute because of the zero axial vector coupling the Z boson to leptons. Therefore, for the $\gamma - Z'$ interference the second bracket in Eq. 3.20 is positive if $g_{Vl} < 0$. For $Z - Z'$ interference this term is given by

$$(g^l_{VZ} g^l_{VZ'} + g^l_{AZ} g^l_{AZ'}) = \Big((\sin^2\theta_w \frac{e}{\sin\theta_w \cos\theta_w})(g_{Vl}) + (-\frac{1}{2}\frac{e}{\sin\theta_w \cos\theta_w})(g_{Al}) \Big). \tag{3.23}$$

It is positive if $g_{Al} < 2\sin^2\theta_w g_{Vl}$. E.g. for a vector coupling or coupling to only left handed leptons it is positive, whereas for coupling to only right handed leptons it is negative.

Fig. 3.3 shows two examples of this behaviour for down quarks in the initial state. The plot displays the interference terms $Z - Z'$ and $\gamma - Z'$, the Z' signal without interference and the sum of them all which is the Z' signal with interference

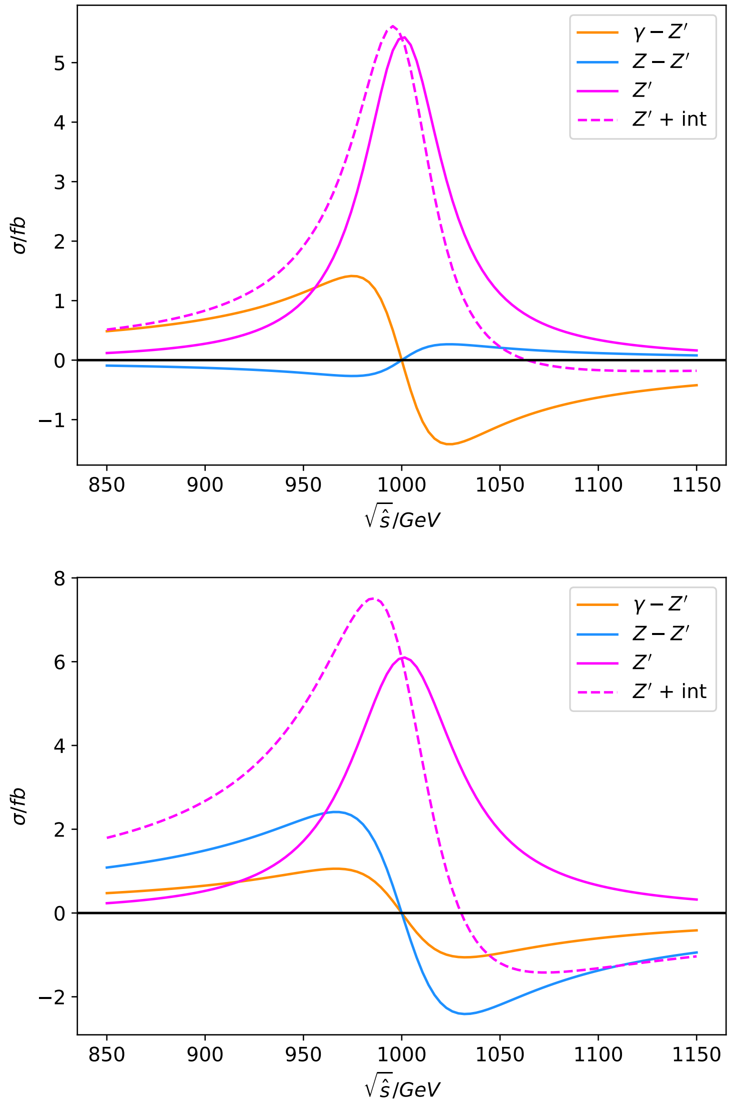

Figure 3.3.: Z' resonance peak and interference terms $Z - Z'$ and $\gamma - Z'$ for vector coupling (above) and coupling only to right handed fermions (below). A negative cross section reduces the Standard Model Drell-Yan process cross section.

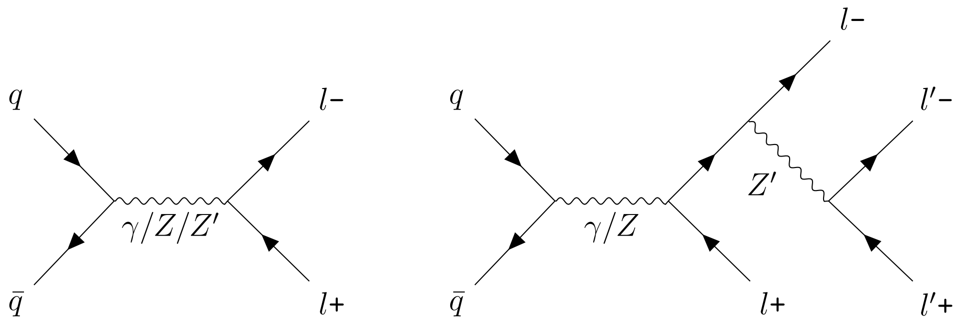

Figure 3.4.: Typical search topologies for Z' at hadron colliders in leptonic final states.

effects. A vectorial (V) and a right handed coupling (R) is contrasted in the two plots. As discussed above, the first term of the $\gamma - Z'$ coupling structure is is positive for $\sum g_{Vl} > 0$ and the second term is positive for $g_{Vl} < 0$. Therefore, the overall coupling structure is negative, since $\sum g_{Vl} > 0$ and $g_{Vl} > 0$ for the V and R model. Therefore, the $\gamma - Z'$ interference term in Fig. 3.3 is flipped for both plots compared to Fig. 3.1, which depicts the kinematical behaviour of the interference term. Similarly, the $Z - Z'$ interference term can be analysed. As discussed above, the first term of the coupling structure for the $Z - Z'$ is positive for $\sum g_{Vl} > 0$. The sign of the second term depends on the model, as discussed below Eq. 3.23. For the V model $g_{Al} < 2\sin^2\theta_w g_{Vl}$ is true, which gives a positive sign of Eq. 3.23. Thus, the overall coupling structure is positive in the V model. Therefore, the interference term in Fig. 3.3 is as depicted in Fig. 3.1. For the R model $g_{Al} < 2\sin^2\theta_w g_{Vl}$ is not true, giving an negative coupling structure. Therefore, the interference term is flipped compared to Fig. 3.1.

3.3. Search strategy

The Large Hadron Collider (LHC) is currently the accelerator with the highest center of mass energy, thus having the highest mass reach to search for particles beyond the Standard Model. Leptonic final states are experimentally clean and therefore, best suited for searches. Two typical search channels for Z' with leptonic final states at hadron colliders are depicted in Fig. 3.4. Searches in the Drell-Yan process, depicted in the diagram on the left in Fig. 3.4, require a coupling of the Z' boson to quarks. In this channel, searches look either for resonant production of Z' bosons or set limits on contact interactions in an effective field theory approach (non-resonance searches). See [19] and [20] for a high and low mass resonance search, and [21] for a non-resonance search of the CMS collaboration. Both search types measure the momenta of the two oppositely charged leptons, p_1 and p_2, and calculate their invariant mass via

$$m_{ll} = (p_1 + p_2)^2. \tag{3.24}$$

The m_{ll} distribution of the SM peaks at the mass of the Z boson and has an falling background from the γ mediated process. For a Z' boson, the m_{ll} distribution peaks at the Z' mass, although this peak can be shifted by interference effects as discussed in the previous section. The diagram on the right in Fig. 3.4 depicts a search channel sensitive to leptophilic Z' models, where the mediator couples only to leptons. A search in the four muon final state for a Z' gauge boson of the $L_\mu - L_\tau$ model is performed in [22]. This search channel is limited to a low mass region for the new boson, since the production cross section is limited by the momentum of the lepton which emits the boson. The aforementioned search focuses on the mass region between 5 and 70 GeV. As discussed in section 3.1, the RGE induces couplings to quarks in the considered simplified Z' model. Therefore, a heavy leptophilic Z' boson can be studied in the Drell-Yan process at the LHC.

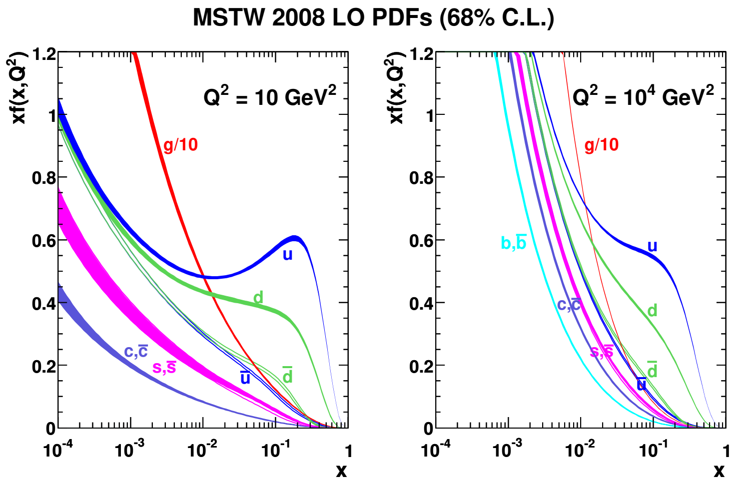

Figure 3.5.: Parton distribution functions $xf_i(x, Q^2)$ for two different energy scales. From [23].

3.4. Drell-Yan process at the LHC

At hadron colliders, the initial particles are protons. If the center of mass energy of the colliding particles is much larger than 1 GeV (the mass of a proton) the substructure of the protons is accessed. At the LHC the center of mass energy is 13 TeV, thus the scattering occurs between the protons constituents. The probability to encounter a specific constituent i, carrying a momentum fraction x of the proton is described by parton distribution functions (PDFs) $f_i(x, \mu_F^2)$. The factorisation scale μ_F separates the high hard-scale of the scattering from the soft scale in the PDFs. The PDFs are probability density functions, which are obtained from fits to scattering data. The PDFs depend on the energy scale at which the proton is probed. Similarly to the renormalization group equation, introduced in section 2.1.1, the energy dependence of PDFs can be determined by considering higher order contributions. PDFs for two different factorisation scales are shown in Fig. 3.5. The interaction between proton constituents, the hard-scattering event, is calculated with perturbative quantum field theory. The cross section at proton level is given by

$$\sigma(PP \to \bar{l}l) = \sum_{q,\bar{q}} \int_0^1 dx_1 \int_0^1 dx_2 f_q(x_1, \mu_F^2) f_{\bar{q}}(x_2, \mu_F^2) \hat{\sigma}(\mu_F, \mu_R, \bar{q}q \to \bar{l}l), \tag{3.25}$$

where $\hat{\sigma}$ denotes the cross section at parton level. The final result depends on the factorisation scale μ_F and the renormalization scale μ_R in the strong coupling constant. This dependence is reduced by taking higher order contributions into account.

The four momentum of two colliding partons, carrying momentum fractions x_1

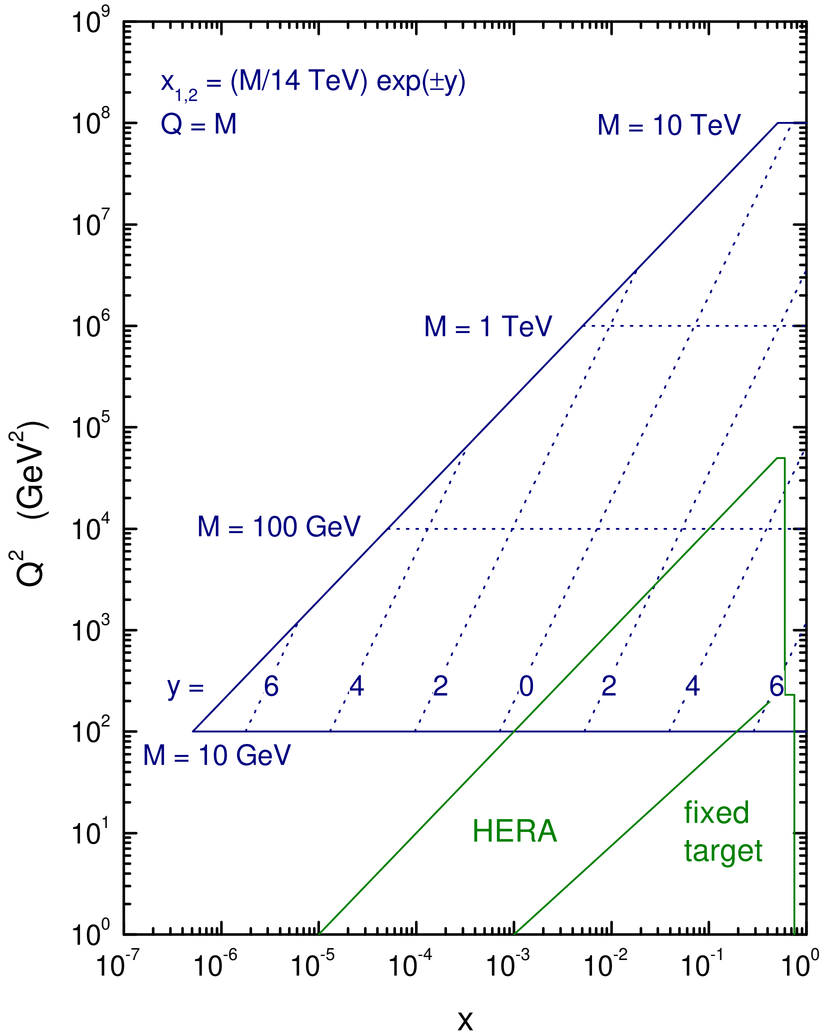

Figure 3.6.: Kinematical properties of the Drell-Yan process at the LHC. From [23].

and x_2 is given by

$$Q = \Big((x_1 + x_2)\sqrt{s}/2, 0, 0, (x_1 - x_2)\sqrt{s}/2\Big). \tag{3.26}$$

Instead of characterising the kinematic properties of the process with x_1 and x_2 it is useful to use the invariant mass M of the resonance and its rapidity y, given by

$$M^2 = Q^2 = x_1 x_2 s \qquad y = \frac{1}{2}\ln\frac{E + p_z}{E - p_z} = \frac{1}{2}\ln\frac{x_1}{x_2}. \tag{3.27}$$

For ultra relativistic particles the rapidity is related to the scattering angle θ via

$$y \approx -\ln\left(\frac{\tan\theta}{2}\right) = \eta. \tag{3.28}$$

η is used to describe the scattering angle at colliders, it is zero for the plane perpendicular to the beam direction. Fig. 3.6 depicts the accessible parameter space, in variables M and y at the LHC. For example, one can read off that a resonance with mass $M = 1$ TeV will have a rapidity smaller than about 3.

3.5. Current Limits

The most stringent limits for the considered model come from the LEP collider. The Large Electron-Positron collider LEP, operating at 209 GeV set limits on contact operators [24]. Limits on leptonic interactions are set at 95% C.L. on the scale Λ, defined by the following effective Lagrangian

$$\mathcal{L}_{\text{eff}} = \frac{g^2}{(1+\delta)(\Lambda^{\eta}_{ff})^2} \sum_{i,j \in L,R} \eta_{ij} \left(\bar{e}_i \gamma_\mu e_i\right) \left(\bar{f}_i \gamma_\mu f_i\right), \tag{3.29}$$

where $\frac{g^2}{4\pi} = 1$ and $\delta = 1(0)$ for electrons (other particles than electrons) in the final state. The limits are set on various interaction structures defined by η_{ij}. The most important ones for what follows, are vector interaction (V) and interactions where only left (L) or right (R) handed particles participate. The Z' interaction Lagrangian in Eq. 3.1 can be cast in the same form

$$\mathcal{L}_{int} = \sum_{l=e,\mu} \left(g_{Ll} \left(\bar{l}_L \gamma_\mu l_L\right) + g_{Rl} \left(\bar{l}_R \gamma_\mu l_R\right) \right) Z'^\mu \tag{3.30}$$

where $g_{R/L} = g_V \pm g_A$. Integrating out the heavy mediator yields an effective description valid for momentum transfers $q^2 << m^2_{Z'}$. For electron contact operators it reads:

$$\begin{aligned} \mathcal{L}_{e\to e} = \frac{1}{m^2_{Z'}} \Big(& g^2_{Le} \left(\bar{e}_L \gamma_\mu e_L\right) \left(\bar{e}_L \gamma^\mu e_L\right) + g_{Le} g_{Re} \left(\bar{e}_L \gamma_\mu e_L\right) \left(\bar{e}_R \gamma^\mu e_R\right) \\ & + g_{Re} g_{Le} \left(\bar{e}_R \gamma_\mu e_R\right) \left(\bar{e}_L \gamma^\mu e_L\right) + g^2_{Re} \left(\bar{e}_R \gamma_\mu e_R\right) \left(\bar{e}_R \gamma^\mu e_R\right) \Big) \end{aligned} \tag{3.31}$$

Matching to Eq. 3.29 yields the limits summarized in Tab. 3.2. Listed are the coupling structure, the coefficients of η_{ij} and the limits from [24]. Similarly, the electron-muon contact operator Lagrangian reads:

$$\begin{aligned} \mathcal{L}_{e\to \mu} = \frac{1}{m^2_{Z'}} \Big(& g_{Le} g_{L\mu} \left(\bar{e}_L \gamma_\mu e_L\right) \left(\bar{\mu}_L \gamma^\mu \mu_L\right) + g_{Le} g_{R\mu} \left(\bar{e}_L \gamma_\mu e_L\right) \left(\bar{\mu}_R \gamma^\mu \mu_R\right) \\ & + g_{Re} g_{L\mu} \left(\bar{e}_R \gamma_\mu e_R\right) \left(\bar{\mu}_L \gamma^\mu \mu_L\right) + g_{Re} g_{L\mu} \left(\bar{e}_R \gamma_\mu e_R\right) \left(\bar{\mu}_R \gamma^\mu \mu_R\right) \Big) \end{aligned} \tag{3.32}$$

Matching to Eq. 3.29 yields the limits summarized in Tab. 3.3. The first (second) letter in the header refers to the coupling structure to electrons (muons). The derived equations in Tab. 3.2 state a linear dependence of the electron couplings to

V	R	L
$\eta_{ij} = 1$	$\eta_{RR} = 1$	$\eta_{LL} = 1$
$g_L = g_V$	$g_R = 2g_V$	$g_L = 2g_V$
$g_{Ve}^2 < \frac{2\pi}{(\Lambda_{ee}^{VV})^2} m_{Z'}^2$	$g_{Ve}^2 < \frac{\pi}{2(\Lambda_{ee}^{RR})^2} m_{Z'}^2$	$g_{Ve}^2 < \frac{\pi}{2(\Lambda_{ee}^{LL})^2} m_{Z'}^2$
$\Lambda_{ee}^{VV} = 20.6$ TeV	$\Lambda_{ee}^{RR} = 8.6$ TeV	$\Lambda_{ee}^{LL} = 8.7$ TeV

Table 3.2.: Limits on couplings to electrons for various coupling structures. In the vector coupling notation the coupling in the L and R model is given by $g_V(1 \pm \gamma^5)$.

VV	RR	RL	LL	LR
$\eta_{ij} = 1$	$\eta_{RR} = 1$	$\eta_{RL} = 1$	$\eta_{LL} = 1$	$\eta_{LR} = 1$
$g_{V\mu} < \frac{4\pi m_{Z'}^2}{g_{Ve}(\Lambda_{\mu\mu}^{VV})^2}$	$g_{V\mu} < \frac{\pi m_{Z'}^2}{g_{Ve}(\Lambda_{\mu\mu}^{RR})^2}$	$g_{V\mu} < \frac{\pi m_{Z'}^2}{g_{Ve}(\Lambda_{\mu\mu}^{RL})^2}$	$g_{V\mu} < \frac{\pi m_{Z'}^2}{g_{Ve}(\Lambda_{\mu\mu}^{LL})^2}$	$g_{V\mu} < \frac{\pi m_{Z'}^2}{g_{Ve}(\Lambda_{\mu\mu}^{LR})^2}$
$\Lambda_{\mu\mu}^{VV} = 18.9$ TeV	$\Lambda_{\mu\mu}^{RR} = 11.6$ TeV	$\Lambda_{\mu\mu}^{RL} = 9.1$ TeV	$\Lambda_{\mu\mu}^{LL} = 12.2$ TeV	$\Lambda_{\mu\mu}^{LR} = 9.1$ TeV

Table 3.3.: Limits on couplings to muons for various coupling structures.

the mediator mass $m_{Z'}$. The limits for muon coupling in Tab. 3.3, for a given electron coupling, depend quadratically on $m_{Z'}$. Fig. 3.7, 3.9 and 3.8 are illustrations of this dependence for the five coupling structures listed in Tab. 3.3. The plots show the maximum allowed coupling to muons as a function of Z' mass and couplings to electrons. The white region is excluded by electron to electron contact interaction. Since the limit on Λ_{ee} is tighter for vectorial interaction, compared to R or L interaction, the boundary to the white region has a smaller slope, and therefore excludes a larger parameter space. The slope is proportional to $1/\Lambda_{ee}$. The colors denote the maximum allowed coupling to muons, given an electron coupling and a Z' mass. The dark blue area denotes the parameter space where muon couplings with values larger than 1 are allowed. Hence no limits on muon couplings are to be respected in this region, since couplings smaller than 1 are assumed for the model. For all of the five coupling structures almost no limits on muon couplings are present for small couplings to electrons. The reason for this is that the initial states at LEP are electrons and positrons. With only small couplings of the Z' boson to the initial states, only little can be inferred about the model, due to the resulting small production cross section. Furthermore, comparing the RR coupling structure with the RL coupling structure, yields the same bounds for the allowed coupling to electrons since the limit is obtained from the same limit on Λ_{ee}^{RR}. But the colored region, denoting the limits on the coupling to muons, is much broader for the RR model. This stems from the tighter limit on $\Lambda_{\mu\mu}^{RR}$ compared to $\Lambda_{\mu\mu}^{RL}$, which constrains the parameter space more. A similar statement can be made about the LL versus the LR model.

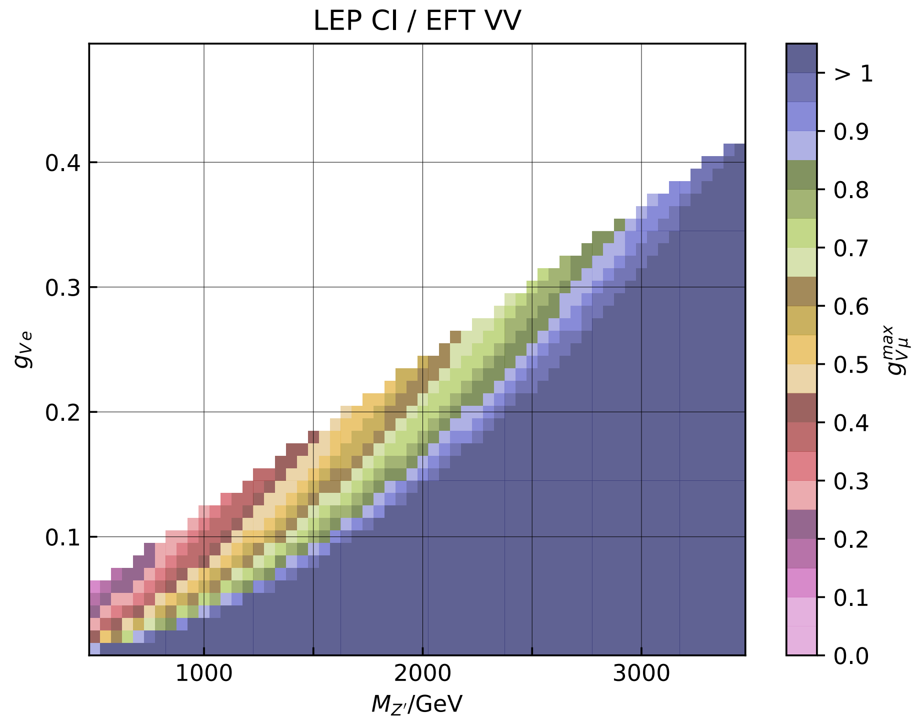

Figure 3.7.: Illustration of the allowed coupling strength of a Z' boson which couples vectorially to electrons and muons. The white region is excluded by the limits on the interaction $\mathcal{L}_{e\to e}$. The color denotes upper limits on g_μ, coming from the interaction $\mathcal{L}_{e\to\mu}$.

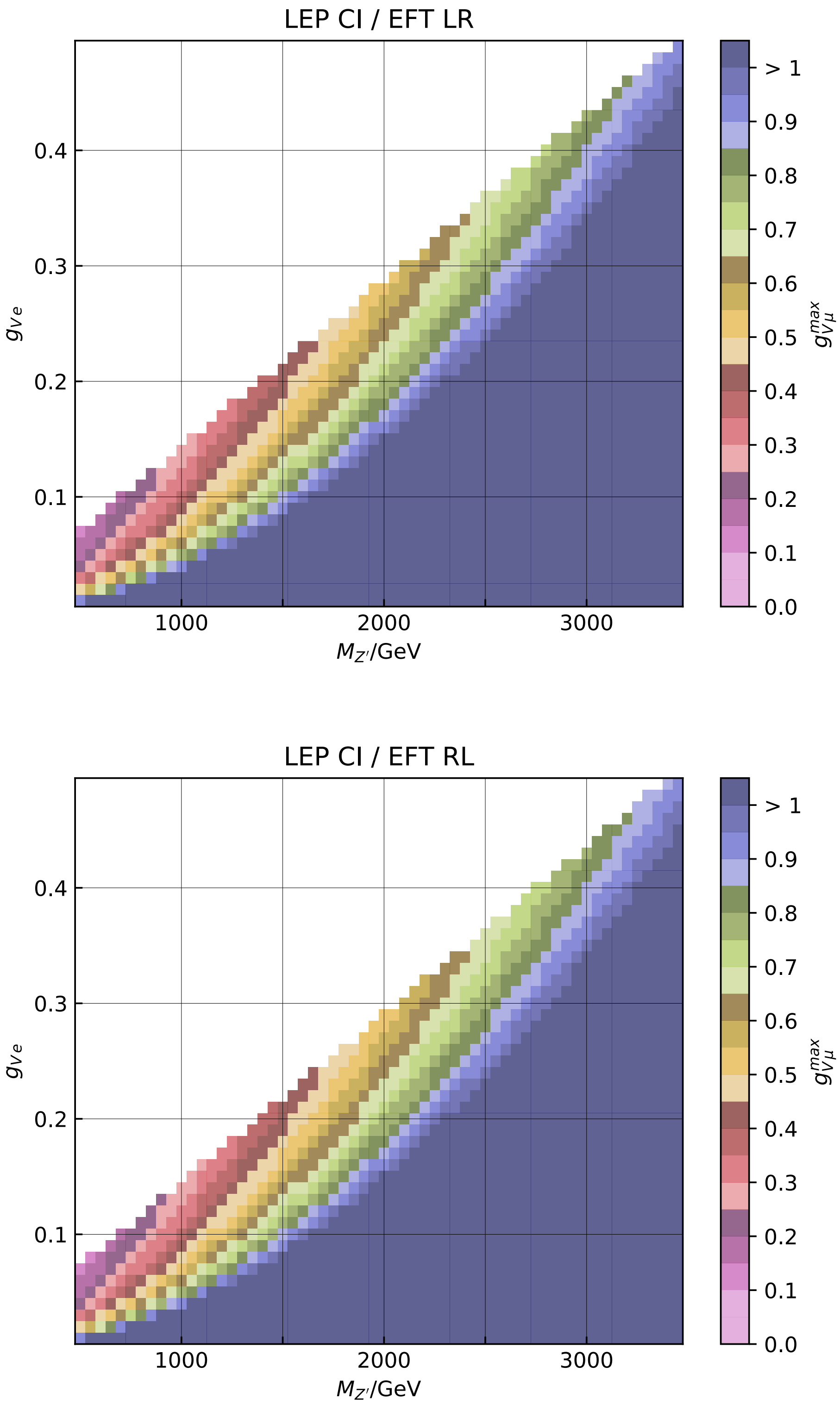

Figure 3.8.: Description as Fig. 3.7. In the figure above (below) only left (right) handed electrons and only right (left) handed muons interact with Z'. In the vector coupling notation the coupling in the L and R model is given by $g_V(1 \pm \gamma^5)$.

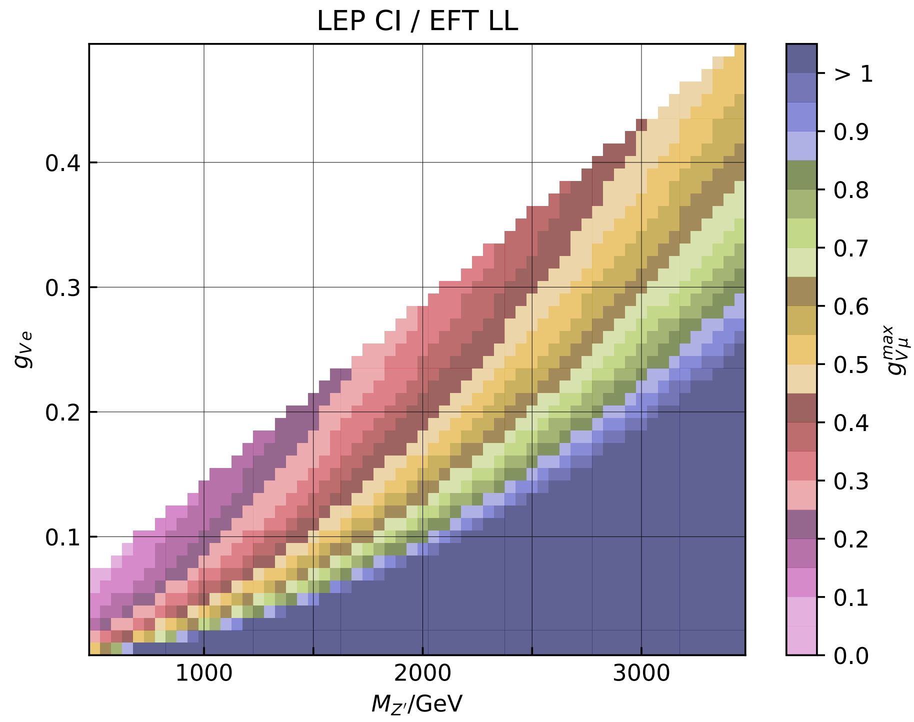

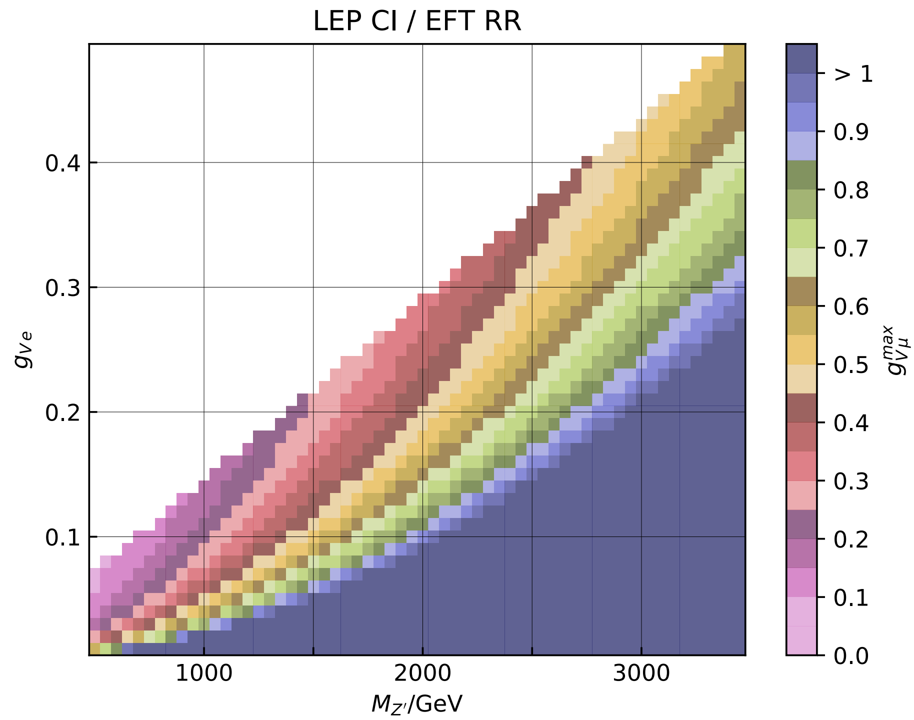

Figure 3.9.: Description as Fig. 3.7. In the figure above (below) only right (left) handed electrons and muons interact with Z'. In the vector coupling notation the coupling in the L and R model is given by $g_V(1 \pm \gamma^5)$.

Furthermore, limits from anomalous magnetic moment measurements and $Z - Z'$ mixing are to be considered. This follows the discussion of the paper where the model was proposed [3]. A Z' boson coupling to leptons contributes to the theory prediction of the anomalous magnetic moment via the following diagram:

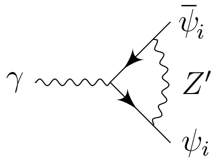

(3.33)

The additional contribution to the SM prediction is given by [25]

$$\hat{a}_l^{Z'} = \frac{1}{12\pi^2}\frac{m_l^2}{m_{Z'}^2}(g_{Vl}^2 - 5g_{Al}^2) + \mathcal{O}\Big(\frac{m_l^3}{m_{Z'}^3}\Big). \tag{3.34}$$

The current 3σ discrepancy for the anomalous magnetic moment for muons is given by [25]

$$\Delta a_\mu = a_\mu^{\mathrm{Exp}} - a_\mu^{\mathrm{SM}} = 28.7(8.0) \times 10^{-10}, \tag{3.35}$$

where the uncertainty $\delta a_\mu = (8.0) \times 10^{-10}$ includes theory and experiment. A positive theory contribution therefore improves the agreement. From the above considered coupling structures, only the vectorial coupling does so. For the V model, the Z' mass for which the discrepancy vanishes is given by

$$m_{Z'} = \sqrt{\frac{g_V^2}{12\pi^2 \Delta a_\mu}} m_\mu \tag{3.36}$$

which equates to 180 GeV for a coupling strength of $g_V = 1$ and the muon mass $m_\mu = 0.105$ GeV. Therefore, no limits are present for the search presented in the next chapter. For the L and R model the discrepancy increases. Limits can be set by requiring that the contribution should not exceed the current uncertainty on the measurement. Similarly, limits can be obtained for the magnetic moment of the electron. The current uncertainty is given by [25]

$$\delta a_e = 0.8 \times 10^{-12}. \tag{3.37}$$

Although its measurement is more precise, the contribution of the Z' model, given in Eq. 3.34, is suppressed by the lower mass of the electron $m_e^2/m_\mu^2 \approx 2 \times 10^{-5}$. Therefore the limits are weaker by an order of ten, as can be seen from Eq. 3.36 with $m_e = 0.511$ MeV.

In the following, the limits from $Z - Z'$ mixing are discussed. After symmetry breaking the Higgs current can be expanded around the minimum $H = \frac{1}{\sqrt{2}}(0\ v)$. Inserting the covariant derivative in the mass eigenstates basis (Eq. 2.41) yields a mass mixing between the Z' and SM Z , given by

$$c_H Z'^\mu H^\dagger i \overleftrightarrow{D}_\mu H = -c_H \frac{2\cos\theta_w}{g} m_Z^2 Z_\mu Z'^\mu + \ldots \tag{3.38}$$

where g denotes the coupling constant of the $SU(2)_L$ gauge group and $v^2 = \frac{4m_Z^2 \cos^2\theta_w}{g^2}$ has been inserted. Mass mixing is constrained by electroweak precision tests, which gives a limit for the mixing angle $\Theta_{\text{mix}} < 10^{-3}$ [3]. In the small mixing limit the angle is given by

$$\Theta_{\text{mix}} \approx -c_H \frac{\cos\theta_w}{g} \frac{m_Z^2}{m_{Z'}^2 - m_Z^2}. \tag{3.39}$$

In Eq. 3.15 an expression for c_H was given. Expressing the couplings in terms of the mediator mass and the variables gives

$$\sum g_{Vl} = \frac{3\pi}{\alpha_Y} \log \frac{\Lambda_{UV}}{m_{Z'}} \Theta_{\text{mix}} \frac{g}{\cos\theta_w} \frac{m_{Z'}^2 - m_Z^2}{m_Z^2}, \tag{3.40}$$

which gives values bigger than 2 for the search presented in the next chapter. Since only couplings smaller than 1 are considered, no constraints are obtained from $Z-Z'$ mixing. E. g. for $m_{Z'} = 500$ GeV it gives $\sum g_{Vl} = 6.7$, where $\frac{g}{\cos\theta_w} = \frac{g'}{\sin\theta_w} = 0.73$, $\alpha_Y = 10^{-2}$ and $m_Z = 91$ GeV has been used.

4. Analysis

As discussed in section 3.2, the Z' boson would cause a peak, centered at $m_{ll} = m_{Z'}$, in the dilepton invariant mass distribution. Furthermore, the peak is shifted slightly by interference effects. In this chapter the analysis technique for the exclusion of BSM parameter points is introduced. Firstly, the method of obtaining signal and background predictions is reviewed and histograms of the dilepton invariant mass spectrum are shown for various Z' model parameter points. Secondly, the analysis in the m_{ll} distributions and in the ratio of the m_{ll} distributions of the electron and muon channel is explained. This furnishes the method of exclusion of Z' model parameter points.

4.1. Signal and background prediction

In order to constrain models for new physics, predictions have to be obtained for the theory under consideration and the SM. The workflow consists of simulating the hard-scatter process and subsequently performing parton showering, which implies radiation of final state particles (FSR) and initial state particles (ISR). Furthermore, potential colored final states need to be confined in colorless states (hadronisation). These steps can be performed with e.g. MadGraph [26] and Pythia8 [27]. Higher order corrections in the hard-scatter process can be included in a next-to-leading order simulation or by rescaling histograms, obtained from a leading order simulation, by shape dependent k-factors. For hadronic Z production these k-factors can be obtained from FEWZ [28]. Apart from QCD (to NNLO) and EW (to NLO) corrections also the photon induced production is implemented in FEWZ. Additionally to the process, also the detector response needs to be simulated. Delphes [29] provides a framework to perform this for various detectors, such as ATLAS or CMS. It is worth mentioning that Delphes is a simpler detector simulation than the ones deployed by the aforementioned experimental collaborations. For example Delphes does not include Bremsstrahlung effects.
Recently, a different approach has been introduced to circumvent these computationally expensive simulations for searches in the Drell-Yan process. Furthermore, deficiencies in the aforementioned detector simulation are avoided. The code ZPEED - Z' Exclusions from Experimental Data [30], does not rely on Monte Carlos simulations, but deduces higher order effects and detector efficiencies from experimental data of a high-mass resonance search performed by the ATLAS collaboration. It allows for exclusion of BSM parameter space with experimental data collected by the ATLAS collaboration at 139 fb^{-1} [31]. In what follows the approach used in

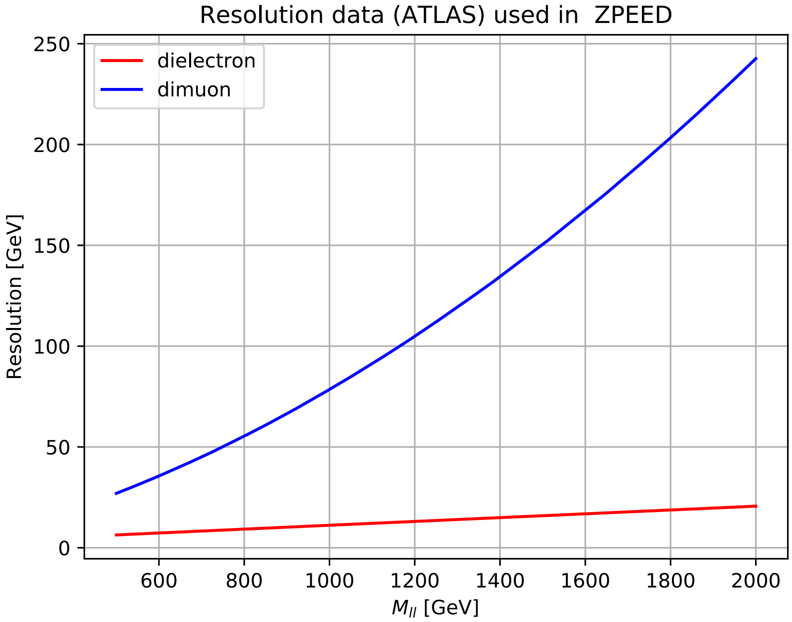

Figure 4.1.: Resolution functions $s(m_{\ell\ell})$ used in ZPEED [30].

ZPEED is reviewed. Details may be found in [30].
The counts measured at the detector in the dilepton channel l in a certain $m_{\ell\ell}$ range for a theory prediction are given by

$$s_i^\ell = \mathcal{L} \int \mathrm{d}m_{\ell\ell}\, \xi_\ell\left(m_{\ell\ell}\right) W_i\left(m_{\ell\ell}\right) \frac{\mathrm{d}\sigma_\ell}{\mathrm{d}m_{\ell\ell}}, \tag{4.1}$$

where $\mathcal{L}$ is the luminosity and $\frac{\mathrm{d}\sigma_\ell}{\mathrm{d}m_{\ell\ell}}$ the differential cross section including parton distribution functions for the theory under consideration. $W_i(m_{\ell\ell})$ encodes the detector resolution per bin. This smearing is modeled with a gaussian kernel and for a bin defined by $m_{\ell\ell} \in [a_i, b_i]$ given by

$$W_i\left(m_{\ell\ell}\right) = \frac{1}{2}\left[\operatorname{erf}\left(\frac{b_i - m_{\ell\ell}}{s\left(m_{\ell\ell}\right)\sqrt{2}}\right) - \operatorname{erf}\left(\frac{a_i - m_{\ell\ell}}{s\left(m_{\ell\ell}\right)\sqrt{2}}\right)\right], \tag{4.2}$$

where $s(m_{\ell\ell})$ denotes the detector resolution. It is taken from auxiliary figures of a ATLAS analysis [31] and depicted in Fig. 4.1. The rescaling factors ξ_ℓ are obtained by $\xi_{\ell,i} = s_{l,i}^{exp}/s_{l,i}^{LO}$. Where $s_{l,i}^{exp}$ refers to the expected counts per bin in the Drell-Yan channel taken from an experimental search [32], while $s_{l,i}^{LO}$ refers to the analytical calculation in Eq. 4.1 with $\xi_\ell = 1$ and the leading order differential cross section $\frac{\mathrm{d}\sigma_\ell}{\mathrm{d}m_{\ell\ell}}$ of the Drell-Yan process. Therefore, the rescaling factors ξ_ℓ encode the selection efficiencies of the experimental search [32] and the higher order corrections to the Drell-Yan process. Tab. 4.1 restates the ξ_ℓ values used in ZPEED. The $m_{\ell\ell}$ values correspond to the bin center. From Tab. 4.1 and Fig. 4.1 it is clear that the

Table 4.1.: Rescaling values ξ_ℓ used in ZPEED. From [30].

$m^i_{\ell\ell}$[GeV]	80	100	185	325	450	600	800	1050	1500	2400	4500
ξ_e	0	0.71	0.88	1.06	1.11	1.11	1.09	1.08	1.06	0.97	0.87
ξ_μ	0	0.56	0.63	0.65	0.65	0.63	0.59	0.59	0.55	0.50	0.51

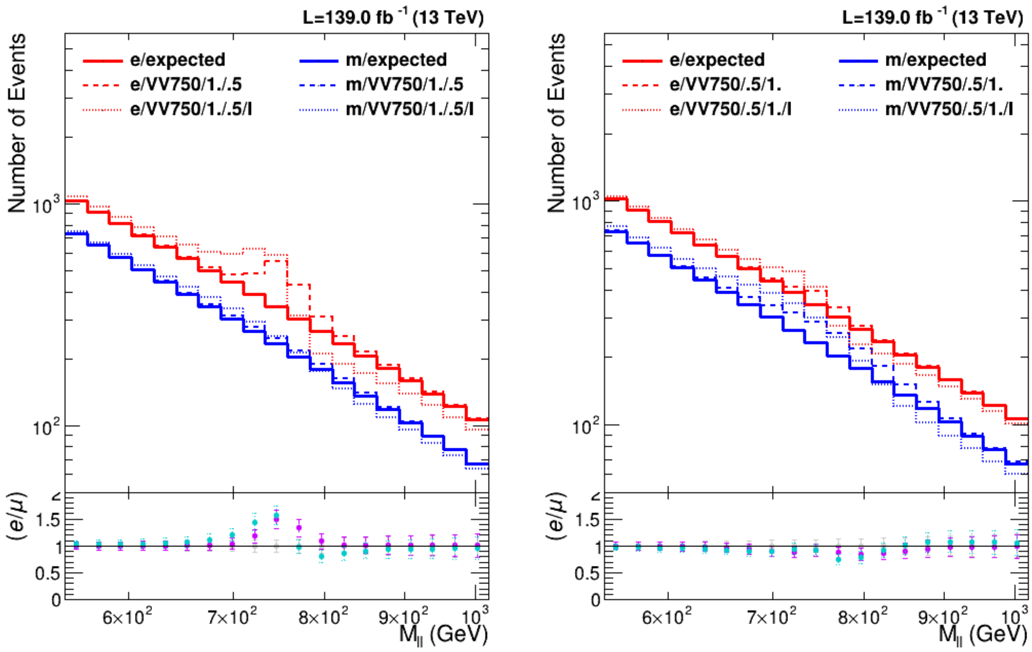

Figure 4.2.: Expected $m_{\ell\ell}$ distributions for SM and leptophilic Z' with $m_{Z'} = 750$ GeV. The width is $\Gamma = 36$ GeV (4.8%) for both cases.

ATLAS search is more sensitive to electrons than to muons. Furthermore, higher order corrections push the ξ_e's to values bigger than 1 in the range $325 - 1500$ GeV. Deploying Eq. 4.1 with the ξ_ℓ function, thus yields a prediction including higher order effects and detector efficiencies. This approach was validated in [30] by obtaining comparable exclusion limits as the ATLAS search for high-mass resonances in the dilepton final state with 139 fb^{-1} [31].

Fig. 4.2 and 4.3 display the expected events for the leptophilic Z' model introduced in chapter 3 for resonance masses of 750 and 1250 GeV. In each figure two cases with vectorial couplings are shown. Both cases depict flavor non-universal couplings to leptons. The histogram on the left shows the model with coupling strengths $g_{Ve} = 1$ and $g_{V\mu} = 0.5$. The SM predictions for the electron (red) and muon (blue) channel are the solid lines. The Z' model predictions without (with) interference effects are represented with dashed (dotted) lines. The interference effects at parton level, separated for initial up- and down type quarks, are discussed in section 3.2. Protons, the initial states at the LHC, consist of both, up- and down type quarks. Therefore, the interference effects at the LHC is a superposition of both, the interference effects

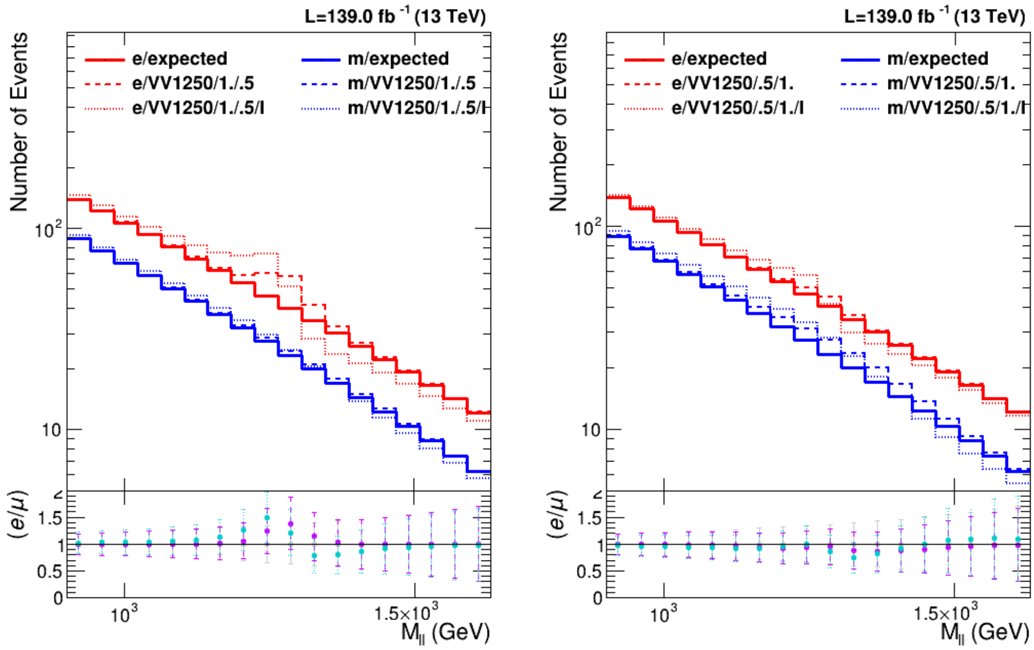

Figure 4.3.: Expected $m_{\ell\ell}$ distributions for SM and leptophilic Z' with $m_{Z'} = 1250$ GeV. The width is $\Gamma = 61$ GeV (4.8%) for both cases.

from initial up- and down type quarks, discussed in section 3.2. From the clearly visible signal peak in the electron channel, the effect of interferences is obvious: including interference effects, shifts the resonance peak and further reduces the prediction below the expected value of the SM for $m_{\ell\ell}$ slightly higher than the resonance mass. Furthermore, the signal with interference effects extends to a much broader $m_{\ell\ell}$ region. This reflects the interference effects at parton level discussed in section 3.2. The histogram also shows the ratio of both channels. It is normalized, such that the SM prediction has a ratio of 1. Also here the differences between omitting and including interference effects (magenta and cyan line respectively) is visible. The histogram on the right shows the reversed situation, where the coupling to electrons is weaker than the couplings to muons $g_{Ve} = 0.5$, $g_{V\mu} = 1$. So the parton level signal of the muon channel in the right histogram is the same as the parton level signal of the electron channel in the left histogram. The signal on the right is much smaller and spread across more bins because of the performance of the ATLAS search in the muon channel, discussed above. The histograms for the resonance mass of 1250 GeV are depicted in Fig. 4.3. Since the induced coupling depends on the low energy scale μ, which is evaluated at the resonance mass, the signals are not as strong as for the 750 GeV case. Furthermore, the lower yields in the bins cause significantly higher statistical uncertainties in the ratios. Fig. 4.4 shows the corresponding histograms with the observed counts in the same mass ranges. The error bars show the statistical uncertainty of each bin.

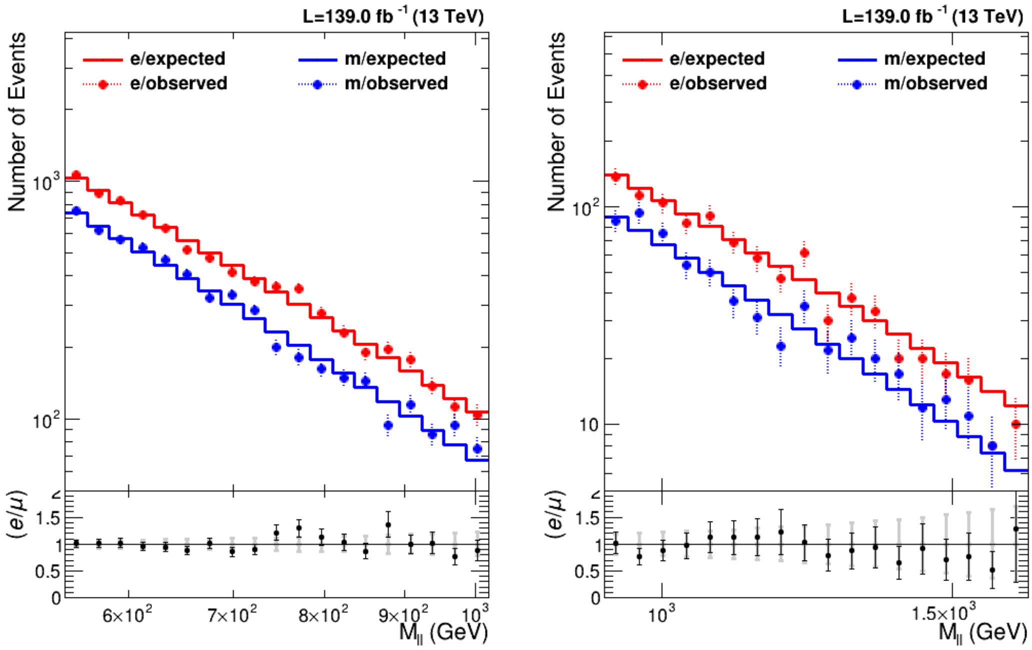

Figure 4.4.: Observed events in dilepton channels around dilepton masses of 750 GeV and 1250 GeV.

4.2. Statistical analysis

Two different types of statistical procedures are considered. Firstly, a resonance search in $m_{\ell\ell}$ bins and secondly a shape analysis in the ratio of the invariant mass spectra of the electron and muon channel. As mentioned in the introduction, the latter is a theoretically cleaner observable, since theoretical uncertainties affecting both channels cancel in the ratio. For example, the choice of the PDF's used for the prediction affects the resulting bin counts. PDFs themselves are obtained from fits to data and are therefore also afflicted with uncertainties. Variations of factorisation and renormalization scales also result in deviations of predictions. Theoretical uncertainties are therefore included in the resonance search.
The resonance search is modeled as N independent counting experiments, each described with a poisson probability distribution. The likelihood function is given by

$$L(\mu) = \prod_{j=1}^{N} \mathrm{Pois}(o_j|\mu s_j + b_j) = \prod_{j=1}^{N} \frac{(\mu s_j + b_j)^{o_j}}{o_j!} e^{-(\mu s_j + b_j)} \tag{4.3}$$

where s_j, (b_j) refers to the Z' signal (Drell-Yan background) counts in bin j, and o_j refers to the observed events from the ATLAS search. The parameter for the poisson distribution of bin j is given by $\mu s_j + b_j$, where μ, the signal strength modifier, is a scaling parameter for the signal hypothesis.

Uncertainties in the background prediction can be incorporated with nuisance parameters. These parameters account for the fact that the true rate may differ from the prediction b_j. In what follows, one nuisance parameter per bin is considered. The predicted background events for bin j are multiplied with the nuisance parameter γ_j, whose nominal value is 1. In the statistical analysis the nuisance parameters are substituted by their maximum likelihood estimate. To limit big deviation of the nuisance parameter from the nominal value a constraint term is multiplied with the likelihood function in Eq. 4.3. The constraint term for γ_j is given by $\mathrm{Pois}(\gamma\sigma_j^{-2}|1\sigma_j^{-2})$, where σ_j denotes the relative uncertainty on the background in bin j. This constraint term can be regarded as a penalty on the negative log likelihood, or in terms of Bayesian statistics as prior of the probability density function of the nuisance parameter [33]. The likelihood function then depends on the signal strength modifier and the nuisance parameters $L(\mu, \gamma_j)$.
For signal hypothesis without interference effects, the signal s_j is directly proportional to the square of Z' couplings to quarks and leptons. Setting a limit on μ therefore translates to a limit on the couplings. The signal hypothesis including interference effects consists of the Z' signal (proportional to the BSM couplings) and the interference term (proportional to BSM and SM couplings). Hence, the proportionality between μ and BSM couplings does not hold. Therefore, no limit is set on μ, but parameter points are excluded if the Z' prediction is not in agreement with the observation.
For the purpose of hypothesis exclusion the signal plus background hypothesis (null) is tested against the background only hypothesis (alternative). For a discovery of a new signal these roles are reversed. The hypothesis test is performed with the $-2\log$ likelihood ratio as test statistic, given by

$$q_\mu = -2\ln\frac{L(\mu, \hat{\theta}_\mu)}{L(\hat{\mu}, \hat{\theta})}. \tag{4.4}$$

$\hat{\mu}$ denotes the maximum Likelihood estimator (MLE) for μ, which maximizes the Likelihood function. If $\hat{\mu} < 0$, then $\hat{\mu} = 0$ is used. θ denotes the set of nuisance parameters. $\hat{\theta}$ also refers to the MLE and $\hat{\theta}_\mu$ to the conditional MLE, given the hypothesis μ. By ignoring nuisance parameters for the moment, it is clear that $\frac{L(\mu)}{L(\hat{\mu})}$ is always ≤ 1 and values close to 1 correspond to a good agreement of observed data and the hypothesis μ. Similarly, q_μ close to 0 reflects this good agreement. To perform the hypothesis test the distribution of q_μ, for background only events (signal plus background events), denoted as $f(q_\mu|\mu = 0)$, $(f(q_\mu|\mu = 1))$ is needed. This can be done by drawing toy data from the probability model defined in Eq. 4.3 and evaluating the test statistic q_μ for the hypothesis under test. Then a normalized histogram from the obtained q_μ values is used as distribution $f(q_\mu|\mu')$ [34]. Note that μ' denotes the value of μ when the toy data are drawn. From the distributions the p values can be calculated via

$$\begin{aligned} p_\mu &= P\left(q_\mu \geq q_\mu^{\text{obs}} | \text{signal} + \text{background}\right) = \int_{q_\mu^{obs}}^{\infty} f\left(q_\mu | \mu, \hat{\theta}_\mu^{obs}\right) dq_\mu \\ 1 - p_b &= P\left(q_\mu \geq q_\mu^{\text{obs}} | \text{background-only}\ \right) = \int_{q_\mu^{\text{obs}}}^{\infty} f\left(q_\mu | 0, \hat{\theta}_0^{obs}\right) dq_\mu, \end{aligned} \tag{4.5}$$

where obs refers to variables obtained from the observed data. The p value denotes the probability to obtain a data sample which is less compatible with the hypothesis compared to the observed sample. From the p values the CLs value is calculated by

$$CL_s(\mu) = \frac{p_\mu}{1 - p_b}. \tag{4.6}$$

If $CL_s \leq 0.05$ the parameter point is excluded at 95% confidence level.

Sampling the distributions of the test statistic is computationally expensive. In Ref. [35] asymptotic formulae are provided for the distributions of the test statistics discussed above. Applying these asymptotic formulae allows for exclusion of BSM parameter points by evaluating an analytical expression. Therefore, the computationally expensive sampling of the distributions of the test statistic is circumvented. The test statistic for the null hypothesis is χ^2, and the alternative hypothesis non-central χ^2 distributed. Fig. 4.5 shows the sampled and asymptotic distributions for one parameter point, where no nuisance parameters have been considered. The p value of the signal plus background hypothesis $p_{\mu=1}$ is the area on the right of q_{obs} of the S+B distribution. Similarly $1 - p_b$ is the area on the right of q_{obs} of the B distribution. The statistical analysis with nuisance parameters is performed with the dedicated tool pyhf [36].
The exclusion of a signal hypothesis in the $m_{\ell\ell}$ ratio is likewise performed with the CLs method. For every bin, the ratio of the counts of the two channels is calculated by $y_j^{obs} = \frac{o_j^e}{o_j^\mu}$ and $y_j^{pred} = \frac{\mu s_j^e + b_j^e}{\mu s_j^\mu + b_j^\mu}$. By neglecting interference and detector effects an estimation of the ratio can be obtained. In this case the signal counts are proportional to the lepton couplings squared $s^l \propto g_l^2$. The signal is also proportional to the couplings to quarks, but this is omitted here, since it affects both channels equally. For small signals, the ratio at the resonance mass can, at leading order in the lepton couplings, be approximated by (setting $\mu = 1$)

$$y^{pred} \approx 1 + k(g_e^2 - g_\mu^2). \tag{4.7}$$

where k is positive and depends on the background counts b and contains all details to calculate the signal counts s, except the lepton couplings. In this approximation the SM gives $y^{pred} = 1$. Thus, as expected, the ratio will be sensitive to highly flavor non-universal parameter points, where g_e and g_μ differ significantly. To perform the hypothesis test the χ^2 function is built

$$\chi^2 = \sum_j \frac{(y_j^{obs} - y_j^{pred})^2}{\sigma_j^2}. \tag{4.8}$$

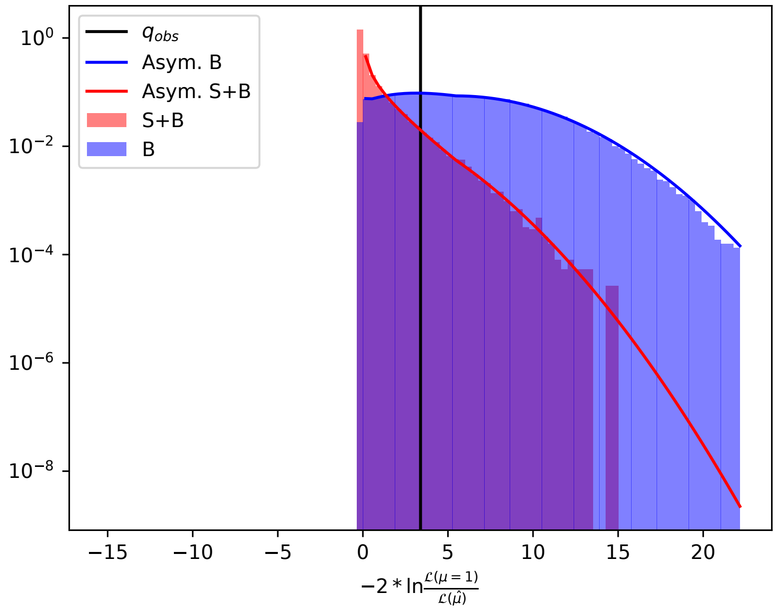

Figure 4.5.: Distribution of the test statistic $q_{\mu=1}$ (Eq. 4.4). Shown are the sampled distributions ($n = 10^5$) and the asymptotic distributions.

This models the y_j values as gaussian distributed. For completeness, it is worth mentioning that the ratio of two poisson distributed quantities does not form a gaussian distribution. Therefore, the statistical model is an approximation. The statistical uncertainty is calculated via gaussian error propagation as

$$\sigma_j = y^{obs}\sqrt{1/o_j^e + 1/o_j^\mu} \rightarrow \sqrt{1/o_j}, \tag{4.9}$$

where the uncertainty of poisson rates $\Delta o = \sqrt{o}$ has been used. Thus, in the high mass region, with less counts, the uncertainty grows as seen in Fig. 4.4. Since the μ dependence in y_j^{pred} is not linear, a different test statistic is used to avoid the maximum Likelihood estimation:

$$q_{\mu=1} = -2\ln\frac{L(\mu=1)}{L(\mu=0)} = -2\ln L(\mu=1) + 2\ln L(\mu=0) = \chi^2(\mu=1) - \chi^2(\mu=0) \tag{4.10}$$

In the asymptotic limit this test statistic gives the same result as the test statistic in Eq. 4.4 [35]. The asymptotic distributions of Eq. 4.10 are gaussian [35], for both, the background only and signal plus background hypothesis. Fig. 4.6 shows the asymptotic and sampled distributions. The observed and the expected test statistics are also shown. The latter is the median of the background only distribution. The evaluation of the CLs value, defined in Eq. 4.6, with the expected value of the test statistic is used to study the sensitivity of an experiment. It quantifies which

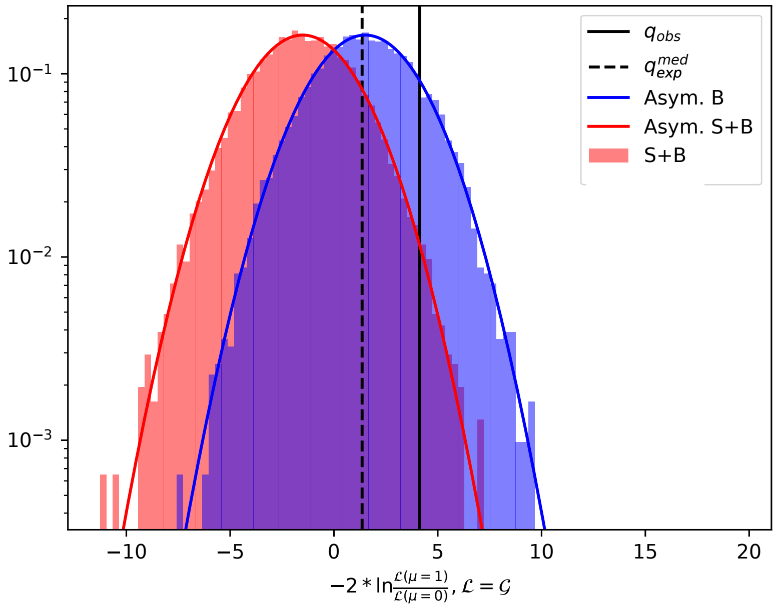

Figure 4.6.: Distribution of the test statistic $q_{\mu=1}$ (Eq. 4.10). Shown are the sampled distributions ($n = 10^5$) and the asymptotic distributions.

parameter points of the BSM model can be excluded, if the data are obtained in the median of the SM distribution. It does not rely on experimental data.

5. Results

In this chapter the analysis outlined in the previous chapter is applied to exclude parameter points of the Z' model. Apart from the introduced leptophilic Z' model, the analysis is also performed on a generic Z' model with tree-level couplings to quarks. The exclusion limits are obtained by restricting the signal region to $m_{\ell\ell} = m_{Z'} \pm 2\Gamma_{\text{eff}}$ [30]. The effective width entails the detector resolution s via $\Gamma_{\text{eff}}^2 = \Gamma^2 + s^2(m_{Z'})$, where Γ is the Z' width. The detector resolution s is depicted in Fig. 4.1. Since the analysis in the ratio of the invariant mass distributions of the electron and muon channel requires the same signal region, the mean resolution of both channels is used to calculate the effective width. The same signal region is chosen for the analysis in m_{ll} distributions to compare the two methods. Two benchmark scenarios for the size of theoretical uncertainties in the m_{ll} distribution are considered: 5% and 15% relative uncertainty per bin as discussed in section 4.2. The exclusion limits of the expected (dashed) and observed (solid) data are shown.

5.1. Leptophilic Z'

The partial width of the Z' boson decaying to a fermion pair is derived in App. C. Summing all decay channels gives the width of the leptophilic Z' boson, defined in Eq. 3.1, by

$$\Gamma_{Z'} = \frac{m_{Z'}}{12\pi} \sum_{l \in e,\mu} (g_V^l)^2 + (g_A^l)^2 + \frac{1}{2}(g_V^l - g_A^l)^2. \tag{5.1}$$

The last term follows from the invisible decay to neutrinos. In what follows vectorial couplings to charged leptons are considered. Couplings to neutrinos are discussed in section 3.1 and given by Eq. 3.2. A parameter point is specified by g_e, g_μ and $m_{Z'}$, where the couplings refer to the vectorial couplings. To study flavor non-universality, exclusion limits are given in the plane spanned by g_e and g_μ for a given resonance mass. The masses are chosen as 500, 750, 1000 and 1250 GeV.
The exclusion limits depicted in Fig. 5.1 are calculated without considering interference effects. The shaded background denotes the radially increasing Z' width in the g_e, g_μ plane, as seen in Eq. 5.1. The broadest resonance, given for couplings of size 1, has a relative width of $\Gamma/m = 7.96\%$. The diagonal in the g_e and g_μ plane corresponds to flavor universal Z' models. Furthermore, straight lines originating from $(0,0)$ connect parameter points with a constant coupling ratio g_μ/g_e. Since the induced couplings to quarks, given in Eq. 3.11, is proportional to $(g_e + g_\mu)$, the Z' production is constant along lines orthogonal to the diagonal representing flavor

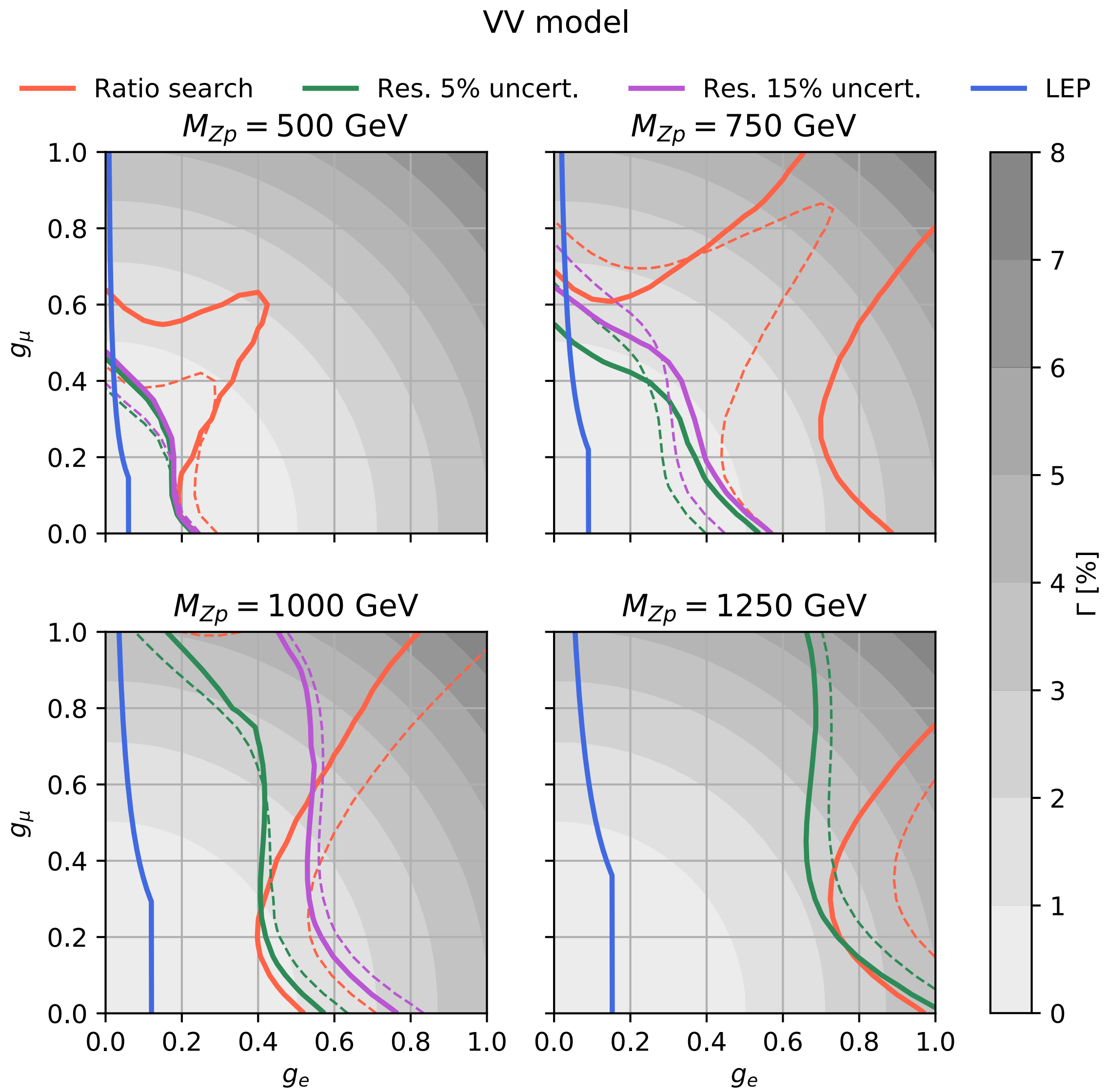

Figure 5.1.: Exclusion plot for the leptophilic Z' model with vectorial couplings to charged leptons without interference effects.

universal models. Furthermore, the production cross section decreases with the resonance mass, since the low energy scale μ of the induced coupling is evaluated at $m_{Z'}$. The relevant term in the induced coupling in Eq. 3.11 is $\log \frac{\Lambda_{UV}}{\mu}$, where Λ_{UV} is set at 10 TeV as discussed in section 3.1.

Limits from LEP (blue) are also shown in the exclusion plot. LEP limits exclude most of the parameter space. Only for small couplings to electrons the LHC is more sensitive. This is because of the vanishing coupling to the initial states at LEP, electrons and positrons, as discussed in section 3.5. The vertical segment of the LEP limit, setting limits on g_e, originates from the $ee \to ee$ scattering process at LEP. The other segment stems from the $ee \to \mu\mu$ channel at LEP and involves both couplings g_e and g_μ. Therefore, it is a curve rather than a straight line in the g_e, g_μ plane.

The sensitivity of the exclusion in the ratio of m_{ll} distributions, discussed in section 4.2, is apparent in Fig. 5.1. For highly flavor non-universal models the expected exclusion line is close to the one obtained by the direct analysis in m_{ll} bins. For flavor universal models the sensitivity of the exclusion in the ratio of m_{ll} distributions decreases, however. The shape in the g_e, g_μ plane resembles the approximate behavior, where detector effects are neglected, of the m_{ll} ratio yielding $1+k(g_e^2-g_\mu^2)$, which was derived in section 4.2.

As mentioned at the beginning of this chapter, the exclusion in the ratio is compared to two exclusions based on m_{ll} distributions with 5% and 15% relative uncertainty per bin. For low resonance masses, the background counts in the Drell-Yan channel are high and the two resonance searches yield approximately the same results. Beginning at a resonance mass of 1000 GeV, the exclusion in the ratio has higher sensitivity than in m_{ll} bins with 15% relative uncertainty for highly flavor non-universal parameter points. For 1250 GeV the analysis in m_{ll} distributions with 15% relative uncertainty cannot exclude any parameter point, whereas the exclusion in the ratio can. The exclusion in m_{ll} bins with 5% relative uncertainty still has higher sensitivity than the ratio for the whole parameter space.

The solid lines represent the exclusion limits based on the observed data by the ATLAS collaboration. The exclusion in the ratio, based on the observations, allows for a bigger exclusion for small g_μ couplings for $m_{Z'} = 1000$ and 1250 GeV compared to the direct analysis in m_{ll} bins with 5% relative uncertainty. This can be understood by looking at the observed counts in Fig. 4.4. For two bins at and slightly lower than 1000 GeV the observed ratio is lower than the SM prediction, and the BSM prediction for the parameter points with $g_e > g_\mu$ predicts a value bigger than the one from the SM prediction. Therefore, strong limits are set on parameter space points with $g_e > g_\mu$. The stronger limit for $m_{Z'} = 1250$ GeV can be interpreted similarly.

Furthermore, the exclusion lines are tighter for electron couplings than for muon couplings. The asymmetry in the g_e, g_μ plane stems solely from the performance difference of the two channels in the ATLAS search on which the signal prediction at detector level relies, as discussed in section 4.1.

Fig. 5.2 shows the same model, but with interference effects taken into account.

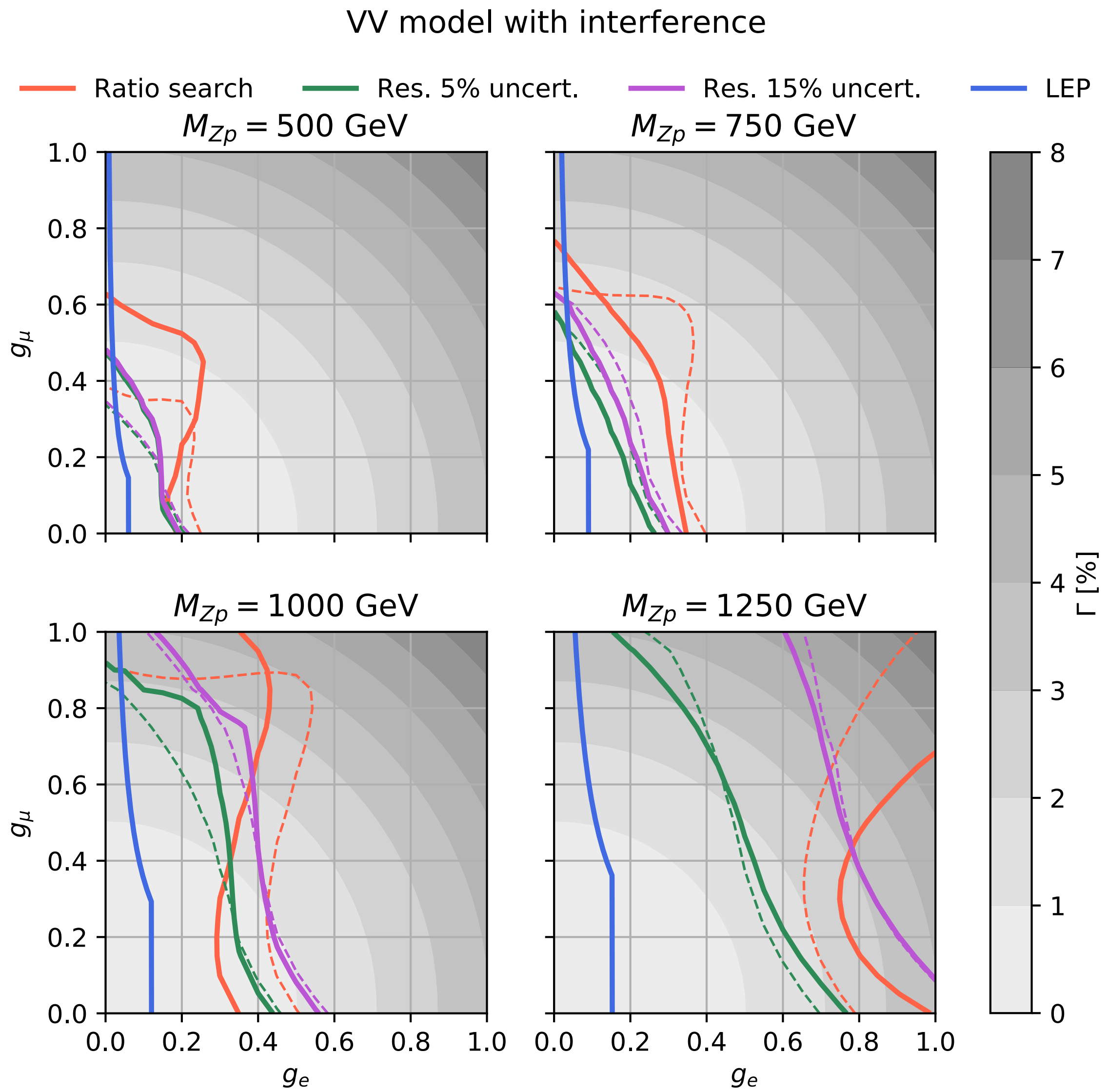

Figure 5.2.: Exclusion plot for the leptophilic Z' model with vectorial couplings to charged leptons with interference effects taken into account.

The behavior is the same as without interference effects, but generally a bigger parameter space can be excluded. For example, the exclusion in m_{ll} bins with 15% relative uncertainty can now also exclude parameter points for $m_{Z'} = 1250$ GeV. As discussed in section 3.2, interference effects increase with the width of the Z' boson, which is proportional to the couplings squared, given in Eq. 5.1. This can also be seen by comparing the exclusion plots in Fig. 5.1 (no interference effects taken into account) and Fig. 5.2 (with interference effects): the exclusion line for $m_{Z'} = 500$ GeV, which is given at small couplings, does not change very much by including interference effects, since the Z' width is small along the BSM parameter points at the exclusion line and consequently also the interference effects. On the other hand, the exclusion line for $m_{Z'} = 1250$ GeV, which is given at large couplings, changes significantly by including interference effects, since the Z' width is large along the BSM parameter points at the exclusion line and therefore also the interference effects. Furthermore, including interference terms improves the sensitivity of exclusion of flavor universal model points, or model points close to flavor universality, as can be seen by comparing Fig. 5.1 and Fig. 5.2. It is worth mentioning that including interference effects not only allows for a better exclusion, but most importantly, should be included since it affects the Z' signal.

5.2. Generic Z'

In this section, the same analysis is performed on a generic Z' model with tree-level couplings to quarks. Hence, the coupling to quarks is not driven by the RGE as for the leptophilic Z' model. A leptophobic model with universal vector couplings to all quark flavors is studied in Ref. [37]. The model is given by the following interaction Lagrangian between the Z' boson and quarks

$$\mathcal{L}_{int} = g_q Z'^{\mu} \Big(\sum_i \bar{u}_i \gamma_\mu u_i + \bar{d}_i \gamma_\mu d_i \Big), \tag{5.2}$$

where the index i denotes the generation of the up and down-type quarks, denoted in Dirac spinor notation. The current limit on g_q for a leptophobic Z', obtained in an analysis of dijet events at the LHC, is at the order of 10^{-1} for the parameter space under consideration [38]. To allow for a signal in leptonic final states, the interaction Lagrangian of the leptophilic Z' model, given in Eq. 3.1, is added to the leptophobic model in Eq. 5.2, resulting in a generic Z' model with tree-level couplings to quarks and leptons. For the studied resonance masses, all six quark flavors are kinematically accessible for the Z' decay. Since quarks carry color charge, the decay to the three color states needs to be included in the width calculation yielding a width given by

$$\Gamma_{Z'} = \frac{m_{Z'}}{12\pi} \Big(3 \times 6 \times g_q^2 + \sum_{l \in e,\mu} (g_V^l)^2 + (g_A^l)^2 + \frac{1}{2}(g_V^l - g_A^l)^2 \Big) \tag{5.3}$$

The first part restates the natural with for the leptophobic Z' given in [38] and the second part concerns decays to leptons and is analogous to the previous section.

Since the following limits to leptons are at the order of 10^{-2} the additional leptonic decay channels have a negligible effect on the width and the branching fraction to quarks. Therefore, the quoted limit $g_q = 10^{-1}$ from the search for a leptophobic Z', given in [38], is studied. The relative width is 0.47%, which can be calculated by using Eq. 5.3.

Fig. 5.3 shows the exclusion limits for the generic Z' model with vectorial couplings to charged leptons and quarks with interference effects taken into account. The rectangular shape in the exclusion line based on the resonance search reflects the independence of both channels, which have been coupled in the leptophilic Z' model by the induced coupling to quarks $\propto g_e + g_\mu$. In the generic Z' model, a change in the g_e coupling does not affect the muon channel. The rounding in the rectangular shape in Fig. 5.3 is the additional gain in sensitivity by combining both channels in one likelihood. To illustrate this gain an additional analysis, in which the likelihood of the electron and muon channel is evaluated separately, is performed. For the separate analysis, for each channel the CLs value is calculated and the lower one of the two is used to test the parameter space for exclusion. Fig. 5.4 compares the, so far deployed combined likelihood analysis (green line) and the separated analysis (magenta line) for the resonance search with 5% relative uncertainty. The exclusion line of the separated analysis does not feature the aforementioned rounding of the combined analysis and therefore does not exclude as many parameter points as the combined analysis. Thus, the gain of sensitivity by combining likelihoods of the channels is apparent. Note that the very small rounding on the edge of the separated analysis is caused by the finite spacing between the evaluated model parameter points. In these figures the performance difference of the ATLAS search in the electron and muon channel, discussed above, is again apparent. Limits on couplings to muons are about twice as large as for electrons. Otherwise the behavior of the exclusion limits is as for the leptophilic Z' model.

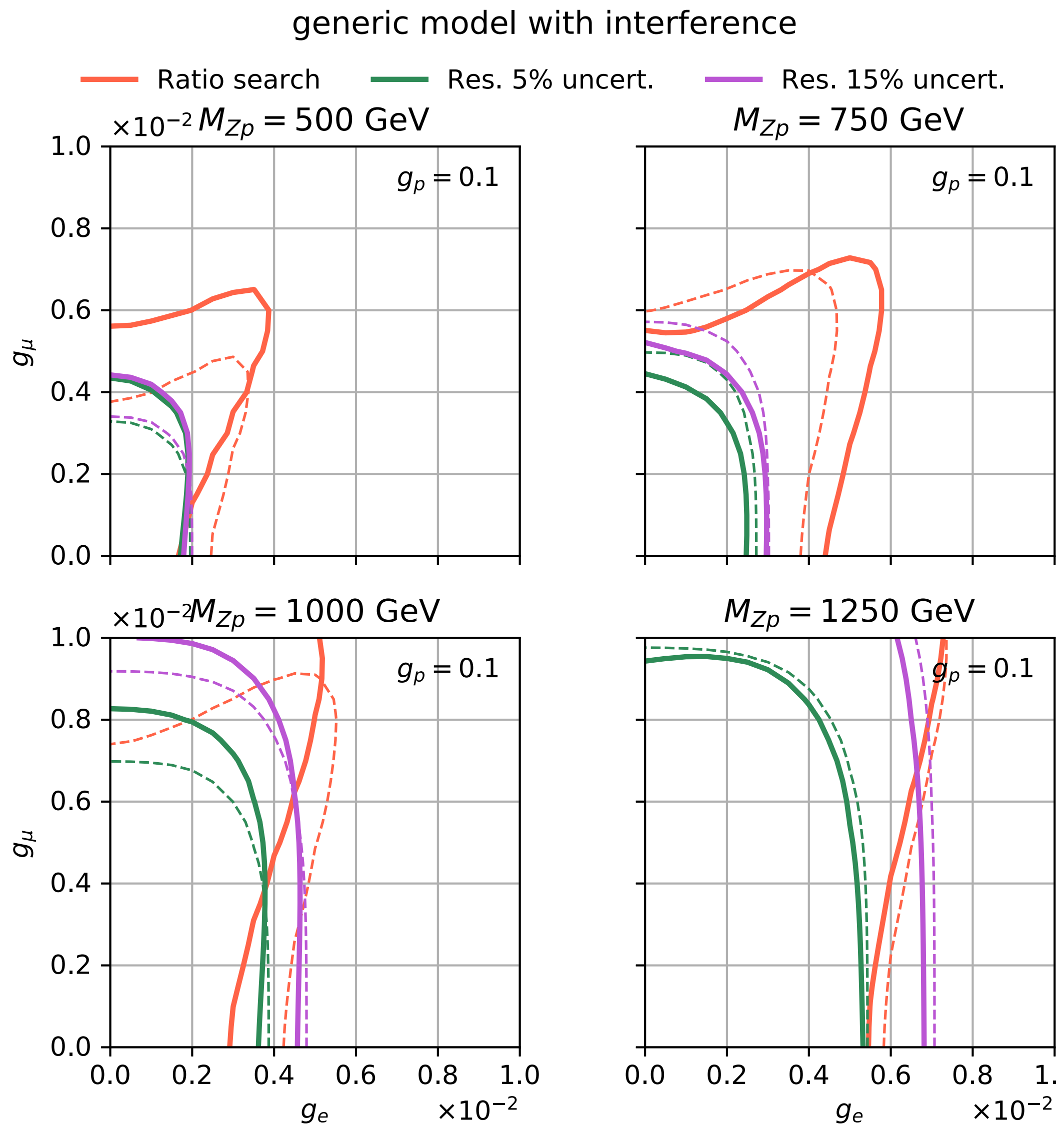

Figure 5.3.: Exclusion plot for the generic Z' model with vectorial couplings to charged leptons and quarks with interference effects taken into account. The relative width is 0.47%.

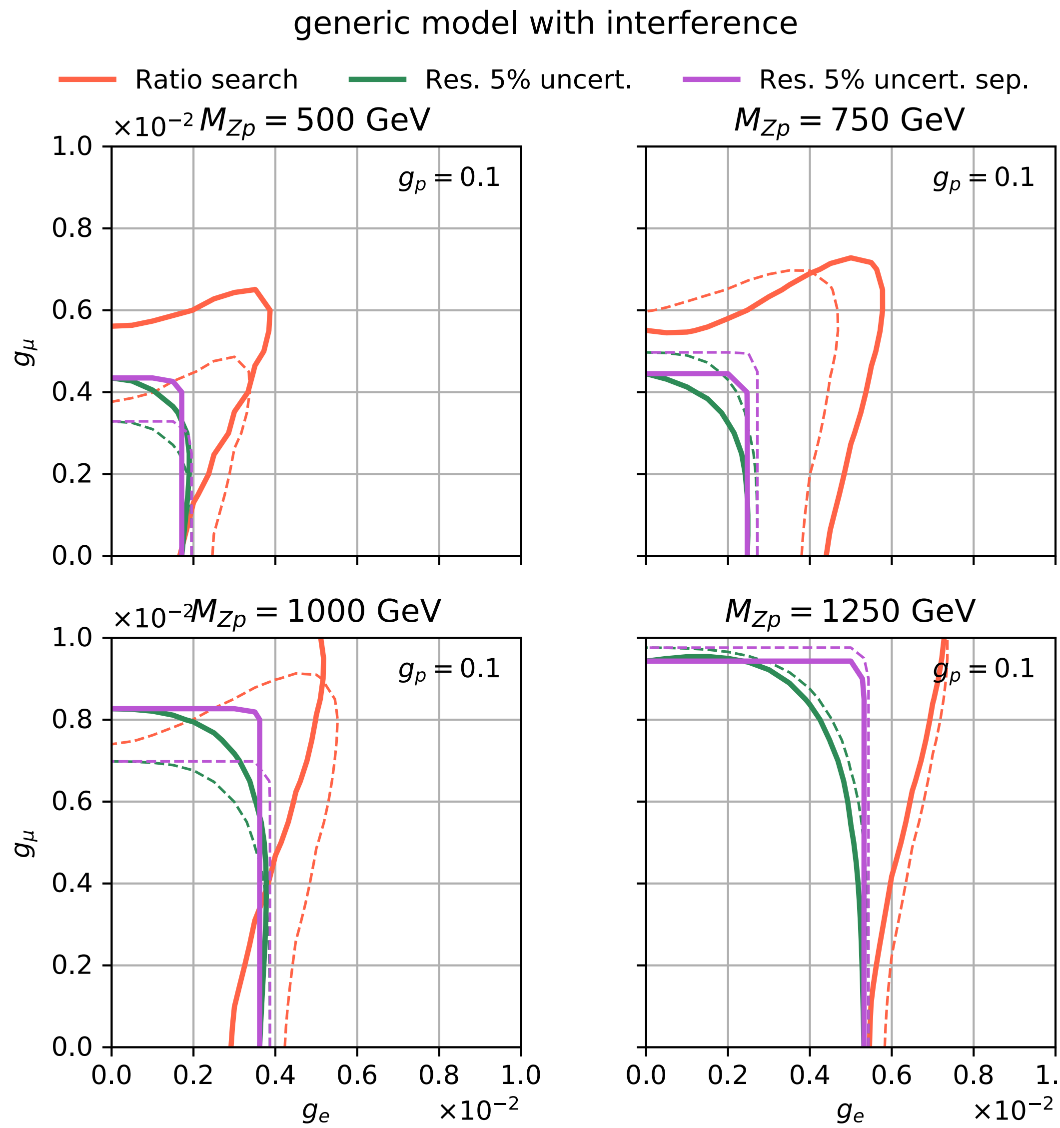

Figure 5.4.: Exclusion plot for the generic Z' model. Combined and separated evaluation of the electron and muon channels in the resonance search is contrasted. The relative width is 0.47%.

6. Conclusion

The Standard Model of particle physics, describing fundamental particles and their interactions except gravity, is measured to a high precision. But there are still observations for which the Standard Model has no explanation and is therefore regarded as being incomplete. This inspires searches for physics beyond the Standard Model. One particular type of extension to the Standard Model are Z' models. In this thesis, a leptophilic Z' model with flavor non-universal couplings, proposed in the context of dark matter searches [3], has been studied. It is a simplified model in which the origin of the Z' mass is not specified. The model is extended by considering couplings to electrons and muons, whereas in the original publication only couplings to a single lepton flavor were studied (μ or τ). No dark matter particle is introduced. Couplings to neutrinos are dictated by the gauge invariance of the Standard Model: neutrinos couple as the left handed component of the charged lepton. The derivation of loop induced couplings was obtained by solving the renormalization group equation. The running of the couplings is driven by hypercharge interactions and induces a coupling of the Z' boson to quarks. Therefore, the leptophilic Z' model can be studied at the LHC.

The importance of interference effects between the Z' boson and the Standard model has been discussed. This topic has not been addressed in the original publication [3]. Interference effects increase with the width of the Z' boson. The consequences of interference effects are a shifted resonance peak and that the signal of the Z' model is not strictly positive. Furthermore, the m_{ll} region in which the signal is detectable is expanded compared to the regular Breit-Wigner resonance shape if interference effects are not taken into account.

Searches at the LHC are complemented by LEP limits on contact operators for Z' bosons coupling to electrons. These limits from LEP are interpreted for the studied Z' model. Electron to electron scattering constrains electron couplings to the Z' boson for a given Z' mass. From limits on electron to muon contact operators, limits for muon couplings for a given electron coupling and resonance mass are derived. This relationship is also graphically presented and discussed.

Signal predictions at the LHC are obtained by deploying the recently published code ZPEED for exclusions in Drell-Yan processes at the LHC. The method, relying on an experimental search from the ATLAS collaboration, is reviewed and ATLAS's higher selection efficiency in this search in the electron than in the muon channel is discussed. Exclusions of Z' model parameter points are obtained with data collected by the ATLAS collaboration at 139 fb^{-1}.

The exclusion in m_{ll} distributions is modelled as independent counting experiments in N bins. Additionally, theoretical uncertainties in the analysis are modeled with

nuisance parameters as per bin relative uncertainties. Two benchmark values of 5% and 15% relative uncertainty are studied. Parameter points are excluded at 95% C.L. with the CLs method.
The statistical evaluation is extended by considering the ratio of electron and muon m_{ll} distributions. This is motivated by the cancellation of theoretical uncertainties in the background prediction. The ratio of m_{ll} distributions is therefore an theoretically cleaner observable. To exclude parameter points, the χ^2 function of the observed and predicted ratios is calculated and a hypothesis test is performed with the CLs method. The exclusion in ratios of m_{ll} distribution is sensitive to highly flavor non-universal parameter points.
Starting at $m_{Z'}$ resonance masses of 1000 GeV the exclusion in the ratio is more sensitive than the exclusion in m_{ll} distribution with 15% relative uncertainty for highly flavor non-universal parameter points. For higher masses the sensitivity of the expected exclusion in m_{ll} bins with 5% relative uncertainty is slightly better, but for the exclusion with the observed data, the exclusion in the ratio of the m_{ll} distribution is slightly better for highly flavor non-universal parameter points.
Finally, the analysis is also applied to a generic Z' model with universal vector couplings to quarks. The quark coupling is set to $g_q = 0.1$, which is the current limit for leptophobic Z' models obtained in dijet searches. In the generic Z' model, the electron and muon channel are independent. This leads to independent exclusion limits for both couplings for the analysis in m_{ll} bins. But combining both channels in one statistical model adds additional sensitivity. This is shown by comparing the combined likelihood of both channels to an analysis where the channels are analysed separately.
In a next step, measurements of the Drell-Yan differential cross sections at the LHC could be analysed and examined if further sensitivity can be gained compared to the present analysis based on a resonance search. Furthermore, a measurement of the ratio of the Drell-Yan differential cross sections would be of interest since it is a theoretically cleaner observable.
The proposed International Linear Collider (ILC), which will collide electrons and positrons at 500 GeV, will further enhance limits on leptophilic models. It will enhance the results from LEP which was operating at 209 GeV. Complementary proposed colliders are the Compact Linear Collider (CLIC), which will collide electrons and positrons at energies up to 3 TeV, and the Future Circular Collider (FCC). The latter could be designed as proton-proton or electron-positron collider. Any of these proposed colliders expands the current reach to discover or constrain BSM models as the Z' model studied in this thesis.

A. Renormalization group equation (RGE)

In this appendix the running of the coupling to the Z' boson is derived. The section starts with the calculation of the loop divergence and further connects to the discussion of the running of the electrical charge in Section 2.1.1. At the end the analytical expression for the running of the leptophilic Z' model, stated in Eq. 3.9 is given.

A.1. Loop calculation

The photon polarization of QED is a special case of the more general boson mixing diagram, where both bosons are the photon. Therefore, the derivation of the general boson mixing diagram is given. The diagram is given by

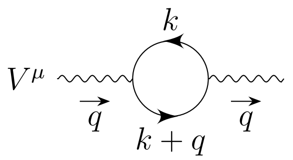

$$= i\Pi^{\mu\nu}(q^2). \qquad \text{(A.1)}$$

The ultraviolet divergent correction is computed in $d = 4 - 2\epsilon$ dimensions. It is best to separate the contributions of couplings to left and right handed fermions in the loop. Assignment of generic couplings:

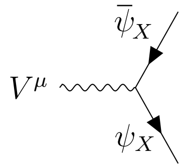

$= ig_X\gamma^\mu$ and

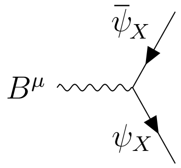

$= ih_X\gamma^\mu$, (A.2)

where $X, Y \in \{R, L\}$. The contributions of the diagram (A.1) is given by

$$i\Pi^{\mu\nu}_{XY} = (-1)\mu^{4-d}\int \frac{dk^d}{(2\pi)^d}\,\mathrm{tr}\left[ig_X\gamma^\mu P_X \frac{i(\not{k}+m)}{k^2-m^2} ih_Y\gamma^\nu P_Y \frac{i(\not{k}+\not{q}+m)}{(k+q)^2-m^2}\right], \qquad \text{(A.3)}$$

where P_X, P_Y denote the corresponding projector

$$P_L = \frac{1-\gamma^5}{2} \quad \text{and} \quad P_R = \frac{1+\gamma^5}{2}. \qquad \text{(A.4)}$$

To evaluate the diagram, the trace needs to be calculated and the momentum shifted.
Denominator:
The substitution $l = k + xq$ leads to a spherical symmetric denominator in l:

$$\frac{1}{(k^2-m^2)((k+q)^2-m^2)} = \int_0^1 dx \frac{1}{(l^2-\Delta)^2}, \tag{A.5}$$

where $\Delta = m^2 - x(1-x)q^2$. The integral measure in Eq. A.3 translates to $\int \frac{dl^d}{(2\pi)^d}$.
Nominator:
Most of the fermion traces equate to zero, the remaining ones are

$$\text{LL:} \rightarrow 2\big(k^\mu(k\cdot q)^\nu + k^\nu(k\cdot q)^\mu - g^{\mu\nu}k\cdot(k+q)\big) - 8ik_\alpha q_\beta \epsilon^{\mu\alpha\nu\beta} \tag{A.6}$$
$$\text{RR:} \rightarrow 2\big(k^\mu(k\cdot q)^\nu + k^\nu(k\cdot q)^\mu - g^{\mu\nu}k\cdot(k+q)\big) + 8ik_\alpha q_\beta \epsilon^{\mu\alpha\nu\beta} \tag{A.7}$$
$$\text{RL=LR:} \rightarrow 2m^2 g^{\mu\nu} \tag{A.8}$$

Where the following trace identities have been used

$$\begin{aligned}
\mathrm{tr}[\gamma^\mu\gamma^\nu] &= 4g^{\mu\nu} \\
\mathrm{tr}[\gamma^\mu\gamma^\nu\gamma^\rho\gamma^\sigma] &= 4(g^{\mu\nu}g^{\rho\sigma} - g^{\mu\rho}g^{\nu\sigma} + g^{\mu\sigma}g^{\nu\rho}) \\
\mathrm{tr}[\gamma^\mu\gamma^\nu\gamma^\rho\gamma^\sigma\gamma^5] &= -4i\epsilon^{\mu\nu\rho\sigma} \\
\mathrm{tr}[\text{odd nr of}\gamma's] &= 0 \\
\mathrm{tr}[(\text{odd nr of}\gamma's)\gamma^5] &= 0 \\
\mathrm{tr}[\gamma^\mu\gamma^\nu\gamma^5] &= 0
\end{aligned} \tag{A.9}$$

The substitution $k = l - xq$ yields the integrands in terms of l. Since the integration boundaries are symmetric, terms $\propto l^\mu$ can be dropped and we use $l^\mu l^\nu = \frac{1}{d}g^{\mu\nu}l^2$. This only affects the LL and RR contribution, which are now equal and given by

$$\text{LL=RR:} \rightarrow 2\Big(-\frac{1}{2}g^{\mu\nu}l^2 + x(1-x)(g^{\mu\nu}q^2 - 2q^\mu q^\nu)\Big). \tag{A.10}$$

The appearing integrals can be expressed with the Γ function, which has poles at zero and negative integer values:

$$\int \frac{dl^d}{(2\pi)^d}\frac{1}{(l^2-\Delta)^2} = \frac{i}{(4\pi)^{d/2}}\frac{\Gamma(2-\frac{d}{2})}{\Delta^{2-d/2}} \tag{A.11}$$
$$\int \frac{dl^d}{(2\pi)^d}\frac{l^2}{(l^2-\Delta)^2} = \frac{-i}{(4\pi)^{d/2}}\frac{\Gamma(1-\frac{d}{2})}{\Delta^{1-d/2}}\frac{d}{2} \tag{A.12}$$
$$= \frac{i}{(4\pi)^{d/2}}\frac{\Gamma(2-\frac{d}{2})}{\Delta^{2-d/2}}2\Delta \tag{A.13}$$

In the second equation the factorial property of the function was used, explicitly: $\Gamma(2-\frac{d}{2}) = (1-\frac{d}{2})\Gamma(1-\frac{d}{2})$. Furthermore, the Γ functions are expanded around its poles using

$$\mu^{4-d}\frac{i}{(4\pi)^{d/2}}\frac{\Gamma(2-\frac{d}{2})}{\Delta^{2-d/2}} = \frac{i}{16\pi^2}\Big(\frac{1}{\epsilon} + \ln\frac{\tilde{\mu}^2}{\Delta} + O(\epsilon)\Big). \tag{A.14}$$

where $\tilde{\mu}^2 = 4\pi e^{-\gamma_E}\mu^2$, and γ_E denotes the Euler-Mascheroni constant. Applying all of these steps yields the final form of the contributions

$$i\Pi^{\mu\nu}_{LL/RR} = \left\{ \begin{array}{c} g_L h_L \\ g_R h_R \end{array} \right\} \int_0^1 dx \frac{-i}{16\pi^2}\left[\frac{1}{\epsilon} + \ln\frac{\tilde{\mu}^2}{\Delta}\right]\left[-2m^2 g^{\mu\nu} + 4x(x-1)\big(2q^\mu q^\nu - g^{\mu\nu}q^2\big)\right] \tag{A.15}$$

$$i\Pi^{\mu\nu}_{LR/RL} = \left\{ \begin{array}{c} g_L h_R \\ g_R h_L \end{array} \right\} \int_0^1 dx \frac{-i}{16\pi^2}\left[\frac{1}{\epsilon} + \ln\frac{\tilde{\mu}^2}{\Delta}\right]\left[+2m^2 g^{\mu\nu}\right] \tag{A.16}$$

In QED, $g_L = g_R = h_L = h_R = -e$, the photon vacuum polarization is given by:

$$\begin{aligned} i\Pi^{\mu\nu} &= i\big(\Pi^{\mu\nu}_{LL} + \Pi^{\mu\nu}_{RR} + \Pi^{\mu\nu}_{LR} + \Pi^{\mu\nu}_{RL}\big) && \text{(A.17)} \\ &= \int_0^1 dx \frac{-ie}{16\pi^2}\left[\frac{1}{\epsilon} + \ln\frac{\tilde{\mu}^2}{\Delta}\right]\left[8x(x-1)\big(2q^\mu q^\nu - g^{\mu\nu}q^2\big)\right] && \text{(A.18)} \end{aligned}$$

To yield the same result as in Eq. 2.28, we can extract the electrical charge and the tensor structure

$$\begin{aligned} i\Pi^{\mu\nu} &= -i\big(g^{\mu\nu}q^2 - q^\mu q^\nu\big)e^2\Pi_2, && \text{(A.19)} \\ \text{where } \Pi_2 &= \frac{1}{2\pi^2}\left[\frac{1}{6\epsilon} + \int_0^1 dx\, x(1-x)\ln\frac{\tilde{\mu}^2}{\Delta}\right]. && \text{(A.20)} \end{aligned}$$

We can further derive the counterterm quoted in section 2.1.1

$$\delta_3 = -e^2\Pi_2(0) = -\frac{e^2}{12\pi^2}\frac{1}{\epsilon} - \frac{e^2}{12\pi^2}\ln\frac{\tilde{\mu}^2}{m^2} \tag{A.21}$$

where the x integration was evaluated easily since at $q = 0$, Δ does not depend on x. Specifically: $\Delta(q = 0) = m^2$.

A.2. RGE for the leptophilic Z' model

In the leptophilic Z' model the mixing of the Z' and B field drives the running of the c_i coupling in $c_i Z'_\mu \bar{\psi}_i \gamma^\mu \psi_i$. The V boson in Eq. A.1 is replaced by the Z' boson with the couplings defined in Eq. 3.1. In left/right handed notation the couplings to a lepton in the loop are given by:

$$g_L = g_{Vl} - g_{Al} \qquad g_R = g_{Vl} + g_{Al} \tag{A.22}$$

The B boson in A.1 denotes now the hypercharge boson. Its coupling to leptons in the loop in the left/right notation are given by

$$h_L = g' y_L \qquad h_R = g' y_R \tag{A.23}$$

Where g' denotes the coupling constant of the $U(1)_Y$ gauge group and y the corresponding hypercharge. The contribution of the electron is given by the sum of the LL, LR, RR, RL part in Eq. A.15:

$$i\Pi_e^{\mu\nu} = \int_0^1 dx \frac{-i}{16\pi^2}\Big[\frac{1}{\epsilon} + \ln\frac{\tilde{\mu}^2}{\Delta}\Big] g' \Big[-2m^2 g^{\mu\nu}\big(2g_{Ae}(y_L - y_R)\big) \tag{A.24}$$

$$+ 4x(x-1)\big(g^{\mu\nu}q^2 - q^\mu q^\nu\big)\big((g_{Ve} - g_{Ae})y_L + (g_{Ve} + g_{Ae})y_R\big)\Big] \tag{A.25}$$

The contribution of the electron neutrino is given by the LL part in Eq. A.15, since there are no right handed neutrinos in the SM:

$$i\Pi_{\nu_e}^{\mu\nu} = \int_0^1 dx \frac{-i}{16\pi^2}\Big[\frac{1}{\epsilon} + \ln\frac{\tilde{\mu}^2}{\Delta}\Big] g' \Big[4x(x-1)\big(g^{\mu\nu}q^2 - q^\mu q^\nu\big)\big((g_{Ve} - g_{Ae})y_L\big)\Big] \tag{A.26}$$

From now on only the $\frac{1}{\epsilon}$ terms are kept, since this is all that is needed for calculating the renormalization group equation (RGE). Note that the mixing takes place before spontaneous symmetry breaking of the Higgs boson. Therefore, the electron has no mass, and the corresponding term is left out. Summing up the electron and electron neutrino contributions yields the contribution of one generation:

$$i\Pi_{1.gen}^{\mu\nu} = \frac{-i}{16\pi^2}\frac{1}{\epsilon}\Big(\frac{-4}{3}\Big) g' \big(g^{\mu\nu}q^2 - q^\mu q^\nu\big)\Big[2(g_{Ve} - g_{Ae})y_L + 1(g_{Ve} + g_{Ae})y_R\Big]. \tag{A.27}$$

The factor of 2 in the term with y_L, compared to the factor of 1 in the term with y_R reflects the symmetry of the unbroken phase: left handed particles come in doublets whereas right handed ones in singlets. Inserting the hypercharges listed in Tab. 2.1 (left handed leptons have $y_L = -\frac{1}{2}$ and right handed leptons have $y_R = -1$.) and extracting the tensor structure, yields

$$i\Pi_{1.gen}^{\mu\nu} = -i\big(g^{\mu\nu}q^2 - q^\mu q^\nu\big)\Pi_{1.gen}, \tag{A.28}$$

$$\text{where } \Pi_{1.gen} = \frac{1}{16\pi^2}\frac{1}{\epsilon}\Big(\frac{8}{3}\Big) g' g_{Ve}. \tag{A.29}$$

With this result at hand the correction due to hypercharge interaction to the operator $c_i Z'_\mu \bar{\psi}_i \gamma^\mu \psi_i$ can be calculated. ψ_i denotes one of the 15 SM fields with definite hypercharge, listed in Table 2.1. The correction is driven by the diagram

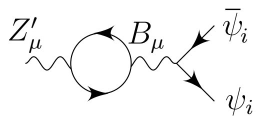

$$= -i\gamma^\mu y_i g' \Pi_{1.gen} \tag{A.30}$$

The propagator of the B field (which is the same as for the photon listed in Sec. 2.1.1), and the tensor structure of $\Pi_{1.gen}^{\mu\nu}$ combine to the projector $g^{\mu\nu} - \frac{q^\mu q^\nu}{q^2}$, where the q term is then dropped. Additional corrections at the same order (α_Y) are given by a B loop in the external ψ fields and a B loop in the vertex. But these contributions have opposite sign and cancel (as in QED) and are therefore not relevant. The tree-level and loop level contribution is given by

$$c_i\Big(1 - \frac{\Pi_{1.gen} g' y_i}{c_i}\Big) Z'_\mu \overline{\psi}_i \gamma^\mu \psi_i = c_i Z_Y Z'_\mu \overline{\psi}_i \gamma^\mu \psi_i, \tag{A.31}$$

where Z_Y has been defined. The RGE is obtained by the scale independence of the bare coupling:

$$\mu \frac{d}{d\mu}(c_i Z_Y) = 0 \rightarrow \mu \frac{d}{d\mu} c_i = -\frac{c_i}{Z_Y} \mu \frac{d}{d\mu} Z_Y \rightarrow \mu \frac{d}{d\mu} c_i = -c_i \mu \frac{d}{d\mu} Z_Y. \tag{A.32}$$

the last line is obtained by considering only leading order. The μ dependence of Z_Y stems from the coupling constant $g'(\mu)$. Inserting the β function for g' at leading order $\mu \frac{d}{d\mu} g' = -\epsilon g'$ [16] in Eq. A.32 yields

$$\mu \frac{d}{d\mu} Z_Y = \frac{1}{c_i} \frac{2}{3\pi} g_{Ve} y_i \alpha_Y, \tag{A.33}$$

where $\alpha_Y = g'^2/4\pi$ has been inserted. This quantity (times -1) is also known as anomalous dimension and abbreviated as γ. Inserting Eq. A.33 in Eq. A.32 yields the order α_Y correction to c_i

$$\mu \frac{d}{d\mu} c_i = -\frac{2}{3\pi} g_{Ve} y_i \alpha_Y \tag{A.34}$$

which can be integrated easily (by neglecting the μ dependence of α_Y)

$$c_i(\mu) = c_i(\Lambda_{UV}) + \frac{2}{3\pi} g_{Ve} y_i \alpha_Y \ln \frac{\Lambda_{UV}}{\mu}. \tag{A.35}$$

Adding the loop contribution of muon and the muon neutrino gives the final result:

$$c_i(\mu) = c_i(\Lambda_{UV}) + \frac{2}{3} \frac{\alpha_Y}{\pi} \Big(\sum_{l \in e,\mu} g_{Vl} \Big) y_i \ln \frac{\Lambda_{UV}}{\mu} \tag{A.36}$$

For completeness also the Z' coupling to the Higgs current is discussed. The Higgs current $H^\dagger i \overleftrightarrow{D}_\mu H = i\Big(H^\dagger (D_\mu H) - (D_\mu H)^\dagger H\Big)$ couples, as the fermions, to the B field with the coupling g' and the hypercharge. This can be seen by solving the e.o.m. for B in the unbroken phase, with gives $\partial^\nu B_{\nu\mu} + g' J^Y_\mu = 0$ [16]. With the hypercharge current defined as

$$J^Y_\mu = \sum_{\psi \in SM} y_\psi \overline{\psi} \gamma_\mu \psi + y_H H^\dagger i \overleftrightarrow{D}_\mu H \tag{A.37}$$

Therefore, the Z' coupling to the Higgs current is given by $c_H Z'^\mu H^\dagger i \overleftrightarrow{D}_\mu H$, as for the Z' coupling to fermions stated at the beginning of this chapter. At tree-level no such term is given in the simplified model, therefore $c_H(\Lambda_{UV}) = 0$. Since the Higgs boson also couples to the fermions in the loop, there are two more diagrams to consider due to Yukawa interaction, depicted here on the right:

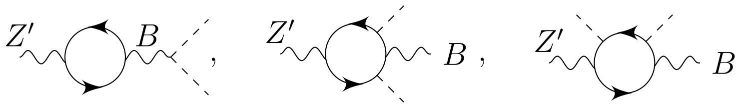

(A.38)

The diagram on the left depicts the hypercharge interaction. The Yukawa interaction diagrams are proportional to the Yukawa couplings squared. The size of the Yukawa coupling can be obtained by inverting $m = \frac{1}{\sqrt{2}}\lambda v$, where m is the mass of the fermion in the loop, λ the corresponding Yukawa coupling and $v = 246$ GeV the vacuum expectation value of the Higgs field. Even for the heavier particle in the loop, the muon ($m_\mu \approx 105$ MeV) , the Yukawa coupling is 0.5×10^{-3}. Therefore, the Yukawa interaction ($\alpha_{Yuk} = \frac{\lambda_\mu^2}{4\pi}$) is negligible compared to the hypercharge interaction since $\alpha_Y \gg \alpha_{Yuk}$ because $\alpha_Y \approx 10^{-2}$, as stated in Eq. 3.13. Inserting the hypercharge for the Higgs boson $y_H = 1/2$ in Eq. A.36 and $c_H(\Lambda_{UV}) = 0$ yields the final result of the running due to hypercharge interactions:

$$c_H(\mu) = \frac{1}{3}\frac{\alpha_Y}{\pi}\Big(\sum_{l\in e,\mu} g_{Vl}\Big)\ln\frac{\Lambda_{\mathrm{UV}}}{\mu}. \tag{A.39}$$

B. Drell-Yan process

In this appendix the cross section for the Drell-Yan process at parton level is calculated. It follows the discussion in [30], which furthermore includes the derivation at hadron level. The contributions are derived for a general Lagrangian, given by

$$\mathcal{L}_{int} = \sum_l V_\mu \, \bar{l}\gamma^\mu(g_V^l + g_A^l\gamma^5)l + V_\mu \, \bar{q}\gamma^\mu(g_V^q + g_A^q\gamma^5)q. \tag{B.1}$$

V_μ refers to a general vector boson, as γ, Z or Z'. The associated Feynman rules are given by

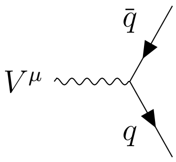

$$= i\gamma^\mu(g_V^q + g_A^q\gamma^5) \quad \text{and}$$

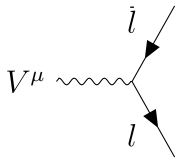

$$= i\gamma^\mu(g_V^l + g_A^l\gamma^5) \tag{B.2}$$

The Feynman diagram for the Drell-Yan process is given by

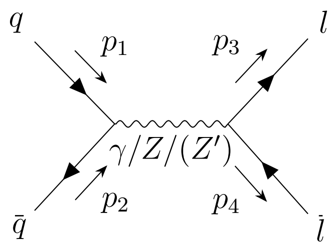

There is also an additional diagram with the Higgs boson in the s-channel. Since fermions have couplings to the Higgs boson that are proportional to their masses, it is negligible for light quarks and leptons. The Drell-Yan process consists of two Standard Model diagrams, with the photon and the Z boson in the s-channel, and the additional Z' diagram. The total amplitude squared is therefore given by:

$$|\bar{\mathcal{M}}|^2 = \sum_{i\in\gamma,Z,Z'} |\bar{\mathcal{M}}_i|^2 + 2 \sum_{i\in\gamma,Z,Z'} \sum_{j\neq i} \Re\left(\overline{\mathcal{M}_i\mathcal{M}_j^*}\right) \tag{B.3}$$

where the bar denotes spin and color average $\frac{1}{2}\frac{1}{2}\frac{1}{N_c}$. The first term refers to squared diagrams, and the second one to interference terms.

The finite widths of the resonances cause an imaginary part in the interference terms, therefore only the real part is considered. It suffices to derive a contribution of one squared diagram and one interference term, since the structure stays the same. For the case of γ the boson mass is zero. The amplitude of a diagram is given by:

$$\mathcal{M}_i = [\bar{v}(p_2)i\gamma^\mu(g_V^q + g_A^q\gamma^5)u(p_1)]\frac{-i\left(g^{\mu\nu} - \frac{k^\mu k^\nu}{m_i^2}\right)}{k^2 - m^2 + im_i\Gamma_i}[\bar{u}(p_3)i\gamma^\nu(g_V^l + g_A^l\gamma^5)v(p_4)] \tag{B.4}$$

where $k = p_1 + p_2$. To form the complex conjugate of the amplitude, the following identities are used:

$$\begin{aligned} \gamma_0^\dagger &= \gamma^0 \qquad \gamma_\mu^\dagger = \gamma^0\gamma_\mu\gamma^0 \qquad \bar{\psi} = \psi^\dagger\gamma^0 \\ \gamma_5^\dagger &= \gamma^5 \qquad 0 = \{\gamma_5, \gamma_\mu\} \end{aligned} \tag{B.5}$$

From which follows

$$\left[\bar{\psi}_1\gamma_\mu\psi_2\right]^* = \left[\bar{\psi}_2\gamma_\mu\psi_1\right] \qquad \left[\bar{\psi}_1\gamma_\mu\gamma_5\psi_2\right]^* = \left[\bar{\psi}_2\gamma_\mu\gamma_5\psi_1\right] \tag{B.6}$$

ad squared diagrams:
After summing over spins the amplitude squared from a single diagram is given by

$$\begin{aligned} |\bar{\mathcal{M}}_i|^2 = &\frac{1}{2}\frac{1}{2}\frac{1}{N_c}\frac{1}{(k^2 - m_i^2)^2 + m_i^2\Gamma_i^2} \\ &\mathrm{tr}\left[\not{p}_2\gamma^\mu(g_V^q + g_A^q\gamma^5)\not{p}_1\gamma^\rho(g_V^q + g_A^q\gamma^5)\right]\mathrm{tr}\left[\not{p}_3\gamma_\mu(g_V^l + g_A^l\gamma^5)\not{p}_4\gamma_\rho(g_V^l + g_A^l\gamma^5)\right] \end{aligned} \tag{B.7}$$

Evaluating the spin traces with the following identities

$$\begin{aligned} \mathrm{tr}[\gamma^\mu\gamma^\nu\gamma^\rho\gamma^\sigma] &= 4(g^{\mu\nu}g^{\rho\sigma} - g^{\mu\rho}g^{\nu\sigma} + g^{\mu\sigma}g^{\nu\rho}) \\ \mathrm{tr}[\gamma^\mu\gamma^\nu\gamma^\rho\gamma^\sigma\gamma^5] &= -4i\epsilon^{\mu\nu\rho\sigma} \end{aligned} \tag{B.8}$$

gives

$$\begin{aligned} |\bar{\mathcal{M}}_i|^2 = &\frac{1}{2}\frac{1}{2}\frac{1}{N_c}\frac{1}{(k^2 - m_i^2)^2 + m_i^2\Gamma_i^2} \\ &\left[4\left((g_V^q)^2 + (g_A^q)^2\right)\left(p_2^\mu p_1^\rho + p_2^\mu p_1^\rho - g^{\mu\rho}(p_1\cdot p_2)\right) - 8ig_A^q g_V^q\epsilon^{\beta\mu\alpha\rho}p_{1\alpha}p_{2\beta}\right] \\ &\left[4\left((g_V^l)^2 + (g_A^l)^2\right)\left(p_{3\mu}p_{4\rho} + p_{3\mu}p_{4\rho} - g_{\mu\rho}(p_4\cdot p_3)\right) - 8ig_A^l g_V^l\epsilon_{\delta\mu\gamma\rho}p_4^\gamma p_3^\delta\right] \end{aligned} \tag{B.9}$$

Contracting the indices and using $\epsilon^{\alpha\beta\mu\nu}\epsilon_{\alpha\beta\rho\sigma} = -2(\delta_\rho^\mu\delta_\sigma^\nu - \delta_\sigma^\mu\delta_\rho^\nu)$ yields

$$\begin{aligned} |\bar{\mathcal{M}}_i|^2 = &\frac{1}{2}\frac{1}{2}\frac{1}{N_c}\frac{1}{(k^2 - m_i^2)^2 + m_i^2\Gamma_i^2} \\ &\left[32\left((g_V^q)^2 + (g_A^q)^2\right)\left((g_V^l)^2 + (g_A^l)^2\right)\left((p_1\cdot p_4)(p_2\cdot p_3) + (p_1\cdot p_3)(p_2\cdot p_4)\right)\right. \\ &\left.+ 128\left(g_V^q g_A^q g_V^l g_A^l\right)\left((p_1\cdot p_4)(p_2\cdot p_3) - (p_1\cdot p_3)(p_2\cdot p_4)\right)\right] \end{aligned} \tag{B.10}$$

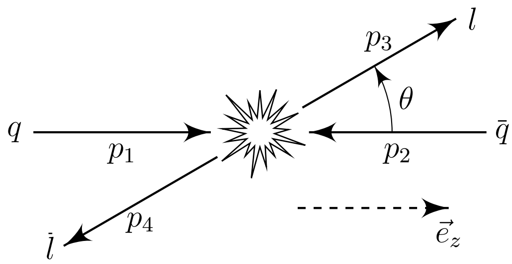

Figure B.1.: Scattering geometry for a 2 to 2 scattering event as the Drell-Yan process.

In the center of mass frame, the four vectors of the (massless) particles are given by

$$p_1 = \frac{\sqrt{\hat{s}}}{2}\begin{pmatrix}1\\ \vec{e}_z\end{pmatrix} p_2 = \frac{\sqrt{\hat{s}}}{2}\begin{pmatrix}1\\ -\vec{e}_z\end{pmatrix} p_3 = \frac{\sqrt{\hat{s}}}{2}\begin{pmatrix}1\\ \vec{e}_f\end{pmatrix} p_4 = \frac{\sqrt{\hat{s}}}{2}\begin{pmatrix}1\\ -\vec{e}_f\end{pmatrix} \tag{B.11}$$

The dot products can be expressed in terms of the scattering angle or the Mandelstam variables:

$$\begin{aligned} \hat{s} &= (p_1+p_2)^2 = 2p_1\cdot p_2 \\ \hat{t} &= (p_1-p_3)^2 = -2p_1\cdot p_3 = -\frac{\hat{s}}{2}(1-\cos\theta) \\ \hat{u} &= (p_1-p_4)^2 = -2p_1\cdot p_4 = -\frac{\hat{s}}{2}(1+\cos\theta) \end{aligned} \tag{B.12}$$

The scattering angle is defined as $\vec{e}_z\cdot\vec{e}_f = \cos\theta$, see Fig. B.1, from which follows

$$(p_1\cdot p_4)(p_2\cdot p_3) + (p_1\cdot p_3)(p_2\cdot p_4) = \frac{2\hat{s}^2}{16}(1+\cos^2\theta) = \frac{\hat{s}^2}{4}(1+2\frac{t}{\hat{s}}+2\frac{t^2}{\hat{s}^2}) \tag{B.13}$$

$$(p_1\cdot p_4)(p_2\cdot p_3) - (p_1\cdot p_3)(p_2\cdot p_4) = \frac{\hat{s}^2}{4}(\cos\theta) = \frac{\hat{s}^2}{4}(1+2\frac{t}{\hat{s}}) \tag{B.14}$$

where in the last equality $\hat{s}+\hat{t}+\hat{u}=0$ was used. Finally, we obtain the amplitude squared

$$\begin{aligned} |\bar{\mathcal{M}_i}|^2 = \frac{1}{2}\frac{1}{2}\frac{1}{N_c}&\frac{\hat{s}^2}{(\hat{s}-m_i^2)^2+m_i^2\Gamma_i^2} \\ &\left[4\Big((g_V^q)^2+(g_A^q)^2\Big)\Big((g_V^l)^2+(g_A^l)^2\Big)(1+\cos^2\theta)+32\Big(g_V^q g_A^q g_V^l g_A^l\Big)(\cos\theta)\right] \end{aligned} \tag{B.15}$$

The differential cross section is given by

$$\frac{d\sigma}{d\Omega} = \frac{1}{64\pi^2\hat{s}}|\overline{\mathcal{M}}|^2 \tag{B.16}$$

which yields

$$\frac{d\sigma}{d\Omega} = \frac{\hat{s}}{256\pi^2 N_c} \frac{1}{(\hat{s}-m_i^2)^2 + m_i^2\Gamma_i^2}$$
$$\left[\left((g_V^q)^2 + (g_A^q)^2\right)\left((g_V^l)^2 + (g_A^l)^2\right)(1+\cos^2\theta) + 8\left(g_V^q g_A^q g_V^l g_A^l\right)(\cos\theta)\right] \tag{B.17}$$

Integrating over the phase space yields the total cross section:

$$\sigma = \frac{1}{12\pi N_c} \frac{\hat{s}}{(\hat{s}-m_i^2)^2 + m_i^2\Gamma_i^2} \left((g_V^q)^2 + (g_A^q)^2\right)\left((g_V^l)^2 + (g_A^l)^2\right) \tag{B.18}$$

The second fraction denotes the kinematical term, depending on $\hat{s}$, and the last part denotes the coupling structure. Alternatively, the differential cross section can be expressed in terms of Mandelstam variables, defined in Eq. B.12

$$\frac{d\sigma}{d\hat{t}} = \frac{2}{\hat{s}} \int d\phi \frac{d\sigma}{d\Omega} \tag{B.19}$$
$$= \frac{1}{8\pi N_c} \frac{1}{\left(\hat{s}-m_i^2\right)^2 + m_i^2\Gamma_i^2} \left[c_0 + c_1\frac{\hat{t}}{\hat{s}} + c_2\frac{\hat{t}^2}{\hat{s}^2}\right] \tag{B.20}$$

where

$$\begin{aligned} c_0 &= \left[(g_V^q)^2 + (g_A^q)^2\right] \cdot \left[\left(g_V^l\right)^2 + \left(g_A^l\right)^2\right] - 4 g_V^q g_A^q g_V^l g_A^l \\ c_1 &= 2c_0 \\ c_2 &= 2\left[(g_V^q)^2 + (g_A^q)^2\right] \cdot \left[\left(g_V^l\right)^2 + \left(g_A^l\right)^2\right] \end{aligned} \tag{B.21}$$

ad interference terms:

The calculation is analog to the one above. The interference term is given by

$$\begin{aligned} \mathcal{M}_i \mathcal{M}_j^* = &= \frac{1}{2}\frac{1}{2}\frac{1}{N_c} \frac{1}{k^2 - m_i^2 + i m_i^2 \Gamma_i^2} \frac{1}{k^2 - m_j^2 + i m_j^2 \Gamma_j^2} \\ &\mathrm{tr}\left[\not{p}_2 \gamma^\mu (g_{Vi}^q + g_{Ai}^q \gamma^5) \not{p}_1 \gamma^\rho (g_{Vj}^q + g_{Aj}^q \gamma^5)\right] \\ &\mathrm{tr}\left[\not{p}_3 \gamma_\mu (g_{Vi}^l + g_{Ai}^l \gamma^5) \not{p}_4 \gamma_\rho (g_{Vj}^l + g_{Aj}^l \gamma^5)\right] \end{aligned} \tag{B.22}$$

which yields

$$\begin{aligned} \frac{d\sigma}{d\Omega} = &\frac{\hat{s}}{256\pi^2 N_c} \frac{\left(\hat{s}-m_i^2\right)\left(\hat{s}-m_j^2\right) + \left(m_i\Gamma_i\right)\left(m_j\Gamma_j\right)}{\left[(\hat{s}-m_i^2)^2 + m_i^2\Gamma_i^2\right]\left[\left(\hat{s}-m_j^2\right)^2 + m_j^2\Gamma_j^2\right]} \\ &\left[4(g_{Vi}^q g_{Vj}^q + g_{Ai}^q g_{Aj}^q)(g_{Vi}^l g_{Vj}^l + g_{Ai}^l g_{Aj}^l)(1+\cos^2\theta)\right. \\ &\left.+ 8(g_{Vi}^q g_{Aj}^q + g_{Vj}^q g_{Ai}^q)(g_{Vi}^l g_{Aj}^l + g_{Vj}^l g_{Ai}^l)(\cos\theta)\right] \end{aligned} \tag{B.23}$$

The total cross section of the interference term is given by integrating over the phase space and yields

$$\begin{aligned} \sigma = &\frac{4}{12\pi N_c} \frac{\left(\hat{s}-m_i^2\right)\left(\hat{s}-m_j^2\right) + \left(m_i\Gamma_i\right)\left(m_j\Gamma_j\right)}{\left[(\hat{s}-m_i^2)^2 + m_i^2\Gamma_i^2\right]\left[\left(\hat{s}-m_j^2\right)^2 + m_j^2\Gamma_j^2\right]} \\ &\left[(g_{Vi}^q g_{Vj}^q + g_{Ai}^q g_{Aj}^q)(g_{Vi}^l g_{Vj}^l + g_{Ai}^l g_{Aj}^l)\right] \end{aligned} \tag{B.24}$$

Where again the second fraction denotes the kinematical term and the last part denotes the coupling structure. The differential cross section in terms of Mandelstam variables reads

$$\frac{d\sigma}{dt} = \frac{1}{8\pi N_c} \frac{\left(\hat{s} - m_i^2\right)\left(\hat{s} - m_j^2\right) + \left(m_i \Gamma_i\right)\left(m_j \Gamma_j\right)}{\left[\left(\hat{s} - m_i^2\right)^2 + m_i^2 \Gamma_i^2\right]\left[\left(\hat{s} - m_j^2\right)^2 + m_j^2 \Gamma_j^2\right]} \left[d_0 + d_1 \frac{\hat{t}}{\hat{s}} + d_2 \frac{\hat{t}^2}{\hat{s}^2}\right] \tag{B.25}$$

where

$$\begin{aligned}
d_0 &= (g^q_{Vi} g^q_{Vj} + g^q_{Ai} g^q_{Aj})(g^l_{Vi} g^l_{Vj} + g^l_{Ai} g^l_{Aj}) - (g^q_{Vi} g^q_{Aj} + g^q_{Vj} g^q_{Ai})(g^l_{Vi} g^l_{Aj} + g^l_{Vj} g^l_{Ai}) \\
d_1 &= 2 d_0 \\
d_2 &= 2(g^q_{Vi} g^q_{Vj} + g^q_{Ai} g^q_{Aj})(g^l_{Vi} g^l_{Vj} + g^l_{Ai} g^l_{Aj})
\end{aligned} \tag{B.26}$$

C. Decay width calculation

The partial decay width of the Z' boson, decaying to the lepton pair $\bar{l}l$ is calculated by evaluating the following diagram:

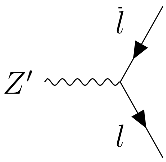

(C.1)

Recycling the trace calculation from Eq. B.9 gives the squared amplitude

$$|\bar{\mathcal{M}}|^2 = \frac{1}{3}\Big[4\Big((g_V^l)^2 + (g_A^l)^2\Big)\Big(p_{3\mu}p_{4\rho} + p_{3\mu}p_{4\rho} - g_{\mu\rho}(p_4 \cdot p_3)\Big)\Big]\Big[-g_{\mu\nu} + \frac{q_\mu q_\nu}{m_{Z'}^2}\Big]. \tag{C.2}$$

The factor of 1/3 reflects the average of the possible states of the massive vector boson. And the last term comes from evaluating the polarization sum $\epsilon_\mu(q)\epsilon^*_\nu(q)$. With the assumption of massless leptons we obtain $p_3 \cdot p_4 = \frac{m_{Z'}^2}{2}$ from momentum conservation. The squared amplitude simplifies to

$$|\bar{\mathcal{M}}|^2 = \frac{4}{3}\Big((g_V^l)^2 + (g_A^l)^2\Big)m_{Z'}^2 \tag{C.3}$$

The partial width is calculated by integrating over the phase space in

$$d\Gamma = \frac{1}{32\pi}|\bar{\mathcal{M}}_i|^2\frac{|\vec{p}_3|}{m_{Z'}^2}d\Omega \tag{C.4}$$

The final result is given by

$$\Gamma_{Z'\to\bar{l}l} = \frac{(g_V^l)^2 + (g_A^l)^2}{12\pi}m_{Z'} \tag{C.5}$$

where $|\vec{p}_3| = \frac{m_{Z'}}{2}$ has been used. The total decay width is given by the sum of all partial decay widths.

List of Figures

List of Tables

Bibliography

[1] **Particle Data Group**, M. Tanabashi *et al.*, "Review of Particle Physics," *Phys. Rev. D* **98** no. 3, (2018) 030001.

[2] **PAMELA** Collaboration, O. Adriani *et al.*, "Ten years of PAMELA in space," *Riv. Nuovo Cim.* **40** no. 10, (2017) 1, `arXiv:1801.10310 [astro-ph.HE]`.

[3] F. D'Eramo, B. J. Kavanagh, and P. Panci, "Probing Leptophilic Dark Sectors with Hadronic Processes," *Phys. Lett. B* **771** (2017) 339–348, `arXiv:1702.00016 [hep-ph]`.

[4] G. Brooijmans *et al.*, "Les Houches 2019 Physics at TeV Colliders: New Physics Working Group Report," in *11th Les Houches Workshop on Physics at TeV Colliders: PhysTeV Les Houches*. 2, 2020. `arXiv:2002.12220 [hep-ph]`.

[5] M. E. Peskin and D. V. Schroeder, *An Introduction to quantum field theory*. Addison-Wesley, Reading, USA, 1995.

[6] M. D. Schwartz, *Quantum Field Theory and the Standard Model*. Cambridge University Press, 2014.

[7] H. Ruegg and M. Ruiz-Altaba, "The Stueckelberg field," *Int. J. Mod. Phys. A* **19** (2004) 3265–3348, `arXiv:hep-th/0304245`.

[8] Wikipedia, "Standard model of elementary particles," 2019. `https://commons.wikimedia.org/wiki/File:Standard_Model_of_Elementary_Particles.svg`. [accessed 01-March-2020].

[9] **CMS** Collaboration, V. Khachatryan *et al.*, "Measurement of the inclusive 3-jet production differential cross section in proton–proton collisions at 7 TeV and determination of the strong coupling constant in the TeV range," *Eur. Phys. J. C* **75** no. 5, (2015) 186, `arXiv:1412.1633 [hep-ex]`.

[10] F. Zwicky, "Die Rotverschiebung von extragalaktischen Nebeln," *Helv. Phys. Acta* **6** (1933) 110–127.

[11] G. Bertone, D. Hooper, and J. Silk, "Particle dark matter: Evidence, candidates and constraints," *Phys. Rept.* **405** (2005) 279–390, `arXiv:hep-ph/0404175`.

[12] **Planck** Collaboration, P. Ade *et al.*, "Planck 2015 results. XIII. Cosmological parameters," *Astron. Astrophys.* **594** (2016) A13, `arXiv:1502.01589 [astro-ph.CO]`.

[13] **Muon g-2** Collaboration, G. Bennett *et al.*, "Final Report of the Muon E821 Anomalous Magnetic Moment Measurement at BNL," *Phys. Rev. D* **73** (2006) 072003, `arXiv:hep-ex/0602035`.

[14] S. Bifani, S. Descotes-Genon, A. Romero Vidal, and M.-H. Schune, "Review of Lepton Universality tests in B decays," *J. Phys. G* **46** no. 2, (2019) 023001, `arXiv:1809.06229 [hep-ex]`.

[15] A. Biekötter, A. Knochel, M. Krämer, D. Liu, and F. Riva, "Vices and virtues of Higgs effective field theories at large energy," *Phys. Rev. D* **91** (2015) 055029, `arXiv:1406.7320 [hep-ph]`.

[16] F. D'Eramo and M. Procura, "Connecting Dark Matter UV Complete Models to Direct Detection Rates via Effective Field Theory," *JHEP* **04** (2015) 054, `arXiv:1411.3342 [hep-ph]`.

[17] B. Allanach, J. Davighi, and S. Melville, "An Anomaly-free Atlas: charting the space of flavour-dependent gauged $U(1)$ extensions of the Standard Model," *JHEP* **02** (2019) 082, `arXiv:1812.04602 [hep-ph]`. [Erratum: JHEP 08, 064 (2019)].

[18] P. Batra, B. A. Dobrescu, and D. Spivak, "Anomaly-free sets of fermions," *J. Math. Phys.* **47** (2006) 082301, `arXiv:hep-ph/0510181`.

[19] **CMS** Collaboration, A. M. Sirunyan *et al.*, "Search for high-mass resonances in dilepton final states in proton-proton collisions at $\sqrt{s} = 13$ TeV," *JHEP* **06** (2018) 120, `arXiv:1803.06292 [hep-ex]`.

[20] **CMS** Collaboration, A. M. Sirunyan *et al.*, "Search for a narrow resonance lighter than 200 GeV decaying to a pair of muons in proton-proton collisions at $\sqrt{s} = 13$ TeV," *Phys. Rev. Lett.* **124** no. 13, (2020) 131802, `arXiv:1912.04776 [hep-ex]`.

[21] **CMS** Collaboration, A. M. Sirunyan *et al.*, "Search for contact interactions and large extra dimensions in the dilepton mass spectra from proton-proton collisions at $\sqrt{s} = 13$ TeV," *JHEP* **04** (2019) 114, `arXiv:1812.10443 [hep-ex]`.

[22] **CMS** Collaboration, A. M. Sirunyan *et al.*, "Search for an $L_\mu - L_\tau$ gauge boson using Z$\rightarrow 4\mu$ events in proton-proton collisions at $\sqrt{s} = 13$ TeV," *Phys. Lett. B* **792** (2019) 345–368, `arXiv:1808.03684 [hep-ex]`.

[23] W. Stirling, "private communication". `https://mstwpdf.hepforge.org/plots/plots.html`. [accessed 01-March-2020].

[24] **ALEPH, DELPHI, L3, OPAL, LEP Electroweak** Collaboration, S. Schael *et al.*, "Electroweak Measurements in Electron-Positron Collisions at W-Boson-Pair Energies at LEP," *Phys. Rept.* **532** (2013) 119–244, `arXiv:1302.3415 [hep-ex]`.

[25] P. Agrawal, Z. Chacko, and C. B. Verhaaren, "Leptophilic Dark Matter and the Anomalous Magnetic Moment of the Muon," *JHEP* **08** (2014) 147, `arXiv:1402.7369 [hep-ph]`.

[26] J. Alwall, R. Frederix, S. Frixione, V. Hirschi, F. Maltoni, O. Mattelaer, H. S. Shao, T. Stelzer, P. Torrielli, and M. Zaro, "The automated computation of tree-level and next-to-leading order differential cross sections, and their matching to parton shower simulations," *JHEP* **07** (2014) 079, `arXiv:1405.0301 [hep-ph]`.

[27] T. Sjöstrand, S. Mrenna, and P. Z. Skands, "A Brief Introduction to PYTHIA 8.1" *Comput. Phys. Commun.* **178** (2008) 852–867, `arXiv:0710.3820 [hep-ph]`.

[28] R. Gavin, Y. Li, F. Petriello, and S. Quackenbush, "FEWZ 2.0: A code for hadronic Z production at next-to-next-to-leading order," *Comput. Phys. Commun.* **182** (2011) 2388–2403, `arXiv:1011.3540 [hep-ph]`.

[29] **DELPHES 3** Collaboration, J. de Favereau, C. Delaere, P. Demin, A. Giammanco, V. Lemaître, A. Mertens, and M. Selvaggi, "DELPHES 3, A modular framework for fast simulation of a generic collider experiment," *JHEP* **02** (2014) 057, `arXiv:1307.6346 [hep-ex]`.

[30] F. Kahlhoefer, A. Mück, S. Schulte, and P. Tunney, "Interference effects in dilepton resonance searches for Z bosons and dark matter mediators," *JHEP* **03** (2020) 104, `arXiv:1912.06374 [hep-ph]`.

[31] **ATLAS** Collaboration, G. Aad *et al.*, "Search for high-mass dilepton resonances using 139 fb^{-1} of pp collision data collected at $\sqrt{s}$ =13 TeV with the ATLAS detector," *Phys. Lett. B* **796** (2019) 68–87, `arXiv:1903.06248 [hep-ex]`.

[32] **ATLAS** Collaboration, M. Aaboud *et al.*, "Search for new high-mass phenomena in the dilepton final state using 36 fb^{-1} of proton-proton collision data at $\sqrt{s} = 13$ TeV with the ATLAS detector," *JHEP* **10** (2017) 182, `arXiv:1707.02424 [hep-ex]`.

[33] J. Conway, "Incorporating Nuisance Parameters in Likelihoods for Multisource Spectra," in *PHYSTAT 2011*, pp. 115–120. 2011. `arXiv:1103.0354 [physics.data-an]`.

[34] ATLAS, CMS, LHC Higgs Combination Group, "Procedure for the LHC Higgs boson search combination in summer 2011," ATL-PHYS-PUB-2011-011, 2011. `http://cds.cern.ch/record/1379837/files/NOTE2011_005.pdf`.

[35] G. Cowan, K. Cranmer, E. Gross, and O. Vitells, "Asymptotic formulae for likelihood-based tests of new physics," *Eur. Phys. J. C* **71** (2011) 1554, `arXiv:1007.1727 [physics.data-an]`. [Erratum: Eur.Phys.J.C 73, 2501 (2013)].

[36] L. Heinrich, M. Feickert, G. Stark, "pyhf: v0.4.1." `https://github.com/scikit-hep/pyhf`.

[37] B. A. Dobrescu and F. Yu, "Coupling-Mass Mapping of Dijet Peak Searches," *Phys. Rev. D* **88** no. 3, (2013) 035021, `arXiv:1306.2629 [hep-ph]`. [Erratum: Phys.Rev.D 90, 079901 (2014)].

[38] **CMS** Collaboration, A. M. Sirunyan *et al.*, "Search for narrow and broad dijet resonances in proton-proton collisions at $\sqrt{s} = 13$ TeV and constraints on dark matter mediators and other new particles," *JHEP* **08** (2018) 130, `arXiv:1806.00843 [hep-ex]`.